Active Noise Control Using Glow Discharge Plasma Panels

by

Christopher Ali Merchant

B.S. Engineering Physics
University of Oklahoma, 1998

Submitted to the Department of Aeronautics and Astronautics
in partial fulfillment of the requirements for a degree of

MASTER OF SCIENCE

At the

MASSACHUSETTS INSTITUTE OF TECHNOLOGY

May 2001

The author hereby grants to MIT permission to reproduce and to distribute publicly
Paper and electronic copies of this thesis document in whole or part

Author .....
Department of Aeronautics and Astronautics
25 May 2001

Certified by .....
John-Paul Clarke
Assistant Professor of Aeronautics and Astronautics, Thesis Supervisor

Accepted by .....
Professor Wallace E. VanderVelde
Chairman, Committee on Graduating Students

Active Noise Control Using Glow Discharge Plasma Panels

by

Christopher Ali Merchant

Submitted to the Department of Aeronautics and Astronautics
on 25 May, 2001 in partial fulfillment of the requirements for the
degree of Master of Science in Aeronautics and Astronautics

Abstract

First-day spacecraft failures frequently occur as a result of the loads experienced during launch into orbit. These loads include structural vibrations transmitted at points of structural contact, and structural-acoustic vibrations created by the excitation of the payload fairing cavity. Structural control techniques, using piezoelectric actuators, have previously been studied as cost-effective ways of reducing the structural-acoustic vibrations being transmitted into the fairing cavity.

These structural control methods, while effective at reducing the sound transmitted into a structure, have not been as effective for controlling acoustic reflections from surfaces. This is due to large impedance mismatches at the solid-fluid interface where control is applied. Recent developments in plasma engineering have made it possible to create a uniform glow-discharge plasma over a surface at one atmosphere (OAUGDP). This creates a thin active layer with almost no impedance mismatch to the surrounding fluid. This thin layer can be used to actuate the air around it much like a speaker.

This thesis investigates the use of thin OAUGDP layer over a surface for active noise control. This technology was also combined with structural control methods to produce a single surface capable of both structural and acoustic actuation. Results from all of these tests indicate an ability to reduce noise by as much as 15.9dB at specific frequencies and by 9dB over a broad frequency range. The reductions were not global in nature, but certain qualities of this control method make it attractive for the problem of reducing acoustic loads on payloads during launch.

Thesis Supervisor: John-Paul Clarke
Assistant Professor of Aeronautics and Astronautics

Acknowledgements

This work was partially supported by the AFOSR Grant No. F49620-96-1-0290 for the purpose of Active Acoustic Launch Load Alleviation. Thanks to Dr. David Miller for initial support of the project,

Special thanks are due to Paul Bauer for suggestions over the last year or so that prevented me from electrocuting myself and others,

Thanks to my lab partner John for his understanding when electricity did go astray,

Thanks to John-Paul Clarke, the best advisor a guy could ask for,

Thanks to various friends in Boston for making the last couple of years enjoyable,

And finally, thanks to my family, especially my parents, Monty and Pamela, for their support of my education over the last twenty odd years.

Contents

List of Figures

List of Tables

Chapter 1

INTRODUCTION

1.1 Motivation

It is estimated that 40% of first-day spacecraft failures occur as a result of the loads experienced during launch into orbit [1]. These loads include structural vibrations transmitted at points of structural contact, and structural-acoustic vibrations created by the excitation of the payload fairing cavity. The structural vibrations are typically reduced by a system of shocks and dampers [2], while the structural-acoustic vibrations are typically reduced by acoustic blankets [3]. The structural-acoustic loads are the greatest at the natural frequencies of both the fairing structure and the acoustic cavity enclosed by the fairing.

Recently, launch operators have shifted from metal to composite payload fairings in an effort to reduce launch weight [4]. This shift has reduced the per-weight cost of launching a payload. The negative effect of the shift is that the less massive composite fairings are actually more susceptible to structural-acoustic vibrations. To compensate, payloads are often over-designed to allow them to survive the harsh launch environment. Much of the savings of lighter payload fairings end up being lost to overly-heavy payloads, or even worse, to missions which fail during launch. All of this has fueled a

search for a way to reduce structural-acoustic vibrations without adding much mass to the system.

Two primary methods exist for reducing these types of vibrations: passive and active. Passive methods involve simply adding mass as a way to reduce vibration. Active methods involve incorporating actuating elements into the structure and controlling these in such a way as to reduce structural excitations.

1.2 Passive Methods

Passive methods include making payload fairings more massive, which runs counter to the desired goal. They also involve application of acoustic blankets to the inside of payload fairings. These blankets are quite dense, and are not very effective at reducing long-wavelength acoustic vibrations unless their thickness is the same order of magnitude as the wavelength to be attenuated. It makes sense to eliminate high-frequency vibrations passively where thin, light blankets can be used, however, it is hoped that low-frequency vibrations could be reduced actively for much less cost in launch weight.

1.3 Active Methods

Active methods for reducing structural-acoustic vibrations have been the focus of study for a number of years [5, 6]. The focus of much of the work has been reducing launch loads, making aircraft cabins quieter, and silencing duct noise. Specifically, there are two primary types of active vibration reduction: Active Noise Control (ANC) and Active Structural-Acoustic Control (ASAC).

Active noise control typically uses a controlled acoustic source, such as a speaker, to cancel noise at a certain location. This is accomplished by sensing the sound present at the location with a microphone, and using the control speaker to apply the opposite pressure wave to that point. Feedback control methods are generally used, although for tonal disturbances, feedforward methods are sometimes employed. ANC can be very effective at reducing sound at a specific point, but is less effective at reducing noise over a large spatial volume. Techniques for global active noise control do exist, but are generally limited to cases when the exact geometry of an enclosure is known.

Active-structural acoustic control has been the focus of much of the previous work at MIT's Space Systems Laboratory as well as at other locations [7, 8]. ASAC methods utilize active elements embedded in a structure to de-vibrate a structure at its natural frequencies. Most previous work has used structurally-bonded piezoelectric patches as actuation sources, with accelerometers and PVDF layers as structural sensors. In efforts to reduce the vibrations caused by broadband, random disturbances, feedback controllers were implemented from these sensors to the PZT patches. Specific frequencies were targeted, and the methods were generally successful at reducing disturbances by as much as 17 dB, or about 80%, at these specific frequencies [9].

Much of the work in ASAC has focused on transmission control, the control of noise being transmitted through a structure. Conversely, ASAC has not been as effective at eliminating reflections from a surface. The primary reason for this is that there is a large impedance mismatch at the solid-fluid interface. This mismatch is apparent in Equation 1, which describes acoustic reflection at a surface [10].

$$\frac{Z_S(\omega)}{Z_F(\omega)} = \frac{1+R}{1-R} \tag{1}$$

Equation 1 shows that when Z_S is much larger than Z_F, the reflection coefficient, R, goes to 1. This represents complete reflection. Applying material properties specific to a thin, aluminum plate [11], we obtain $Z_S \approx 1.73 \times 10^7$, and for air at standard pressure [12], $Z_F \approx 410$. This means that, generally, $Z_S >> Z_F$ so that we can require Equation 2 to be true.

$$\frac{1+R}{1-R} \Rightarrow \infty \therefore R \Rightarrow 1 \tag{2}$$

Equation 2 shows that reflection at the boundary between a solid and a fluid will be complete except at the natural frequencies of the system. It is only at the poles of Z_F and the zeros of Z_S are the impedances close enough that there is not complete reflection at a surface. By implementing a transmission controller on a surface and reducing the poles of Z_S the exit path for interior vibrations is further removed. In this case, sound transmitted into the payload cavity is trapped. A method of removing the trapped interior acoustic energy is required to fully reduce the acoustics of the system.

Because it is very difficult to drive a solid to behave like a fluid, this impedance mismatch occurs regardless of the control scheme used. For this reason, ASAC will always be more effective at reducing transmission through a surface than reflection at a surface. To control reflections at a surface it would be better to have an actuator without an impedance mismatch. One possible combination would be to have an ASAC controller using piezoelectric patches for transmission control and a second controller based on ANC using a fluid-based actuator to reduce noise trapped inside the cavity.

Constraints on the methods used to reduce these vibrations are significant. Due to the high cost of a launch, and more specifically, the cost per payload weight, any method used to reduce vibrations to a payload must be lightweight.

1.4 An Alternative Approach

Finding an alternative to using structural sensor actuator pairs for controlling acoustic reflections is the focus of this work. In an effort to minimize the impedance mismatch between the actuator and the surrounding fluid, it was determined that a fluid-based actuator would be the best choice. It is hoped that such an actuator could be used in conjunction with current structural control methods to further reduce noise inside of a cavity.

Recent work in the plasma science community has resulted in the ability to generate a weakly-ionized, uniform plasma at one atmosphere [13]. Such a plasma is a mixture of positively charged ions and negatively charged electrons, along with a much larger number of neutral air molecules. The acoustic impedance of such a plasma is equal to the impedance of air. The ability to produce a thin layer of this plasma over the interior of the cavity to be controlled provides a method of actuation with almost no impedance mismatch to the surrounding fluid. The design and testing of this approach is the focus of this work.

A control source based on actuating a layer of plasma and interacting with the surrounding air directly would necessarily use ANC control techniques. One limitation of such techniques is that they generally do not produce global attenuations, unlike ASAC methods. To produce global, rather than local, reductions in acoustics is possible

using ANC methods [14]. It requires additional modeling of the problem and an incorporation of modal actuation. It is the hope of this work that such a global actuator can be produced based on the plasma technology discussed in the next section.

1.5 Experimental Approach

The experimental work performed here will follow naturally from previous work on the subject done at MIT. Much of the hardware used will be the same, and many control design techniques will also follow from this work. The reason for this, aside from easing development of new technology, is in order to provide comparable results between past and current work.

While the work here may have other applications to active noise control problems, specific application to the launch loads problem is being considered. For this reason, we will limit frequencies observed to below 500 Hz. This is under the assumption that above 500 Hz, attenuation is handled by passive acoustic blankets. Weight considerations, which are a driving factor behind any spacecraft design will also be studied.

1.6 Thesis Outline

This thesis describes an experimental study of the control of thin layers of plasma to provide active noise control. A benchmark for the noise reductions that might be expected from such a method is determined experimentally. Combining this technology with previous structural control methods is also investigated. The applicability to the launch loads problem is discussed as a possible use for this research. Included in this thesis are:

- One-Atmosphere Uniform Glow Discharge Plasma
- Tone Cancellation Experiment
- Random Disturbance Attenuation Experiment
- Structural-Acoustic Control
- Combined Structural and OAUGDP Control
- Global vs. Local Reductions

Chapter 2

ONE-ATMOSPHERE UNIFORM GLOW DISCHARGE PLASMA

2.1 Background

The ability to produce a uniform, glow-discharge plasma was recently demonstrated by Roth [15] in one-atmosphere conditions (OAUGDP). The technique used is based on the idea of "charge-trapping", and requires alternating electric fields across a volume of gas. The plasma produced is of the low-temperature, weakly-ionized variety and is assumed to be able to interact with the surrounding neutral gas via ion-neutral collisions. The fact that it is produced at one atmosphere means that heavy vacuum equipment is not needed in the plasma generation process, as is usually the case.

The process used to generate an OAUGDP was patented by Roth, and consists of two electrodes separated by a sufficient air gap and a power supply capable of producing high voltages at radio frequencies [16]. Specifically, the power supply was able to produce voltages of up to around 10 kV, at frequencies from 500 Hz to several kHz. Due to power limitations of any such power supply in a laboratory situation, the electrodes were realistically limited in size to about 1 square foot each. The basic setup is shown in Figure 1.

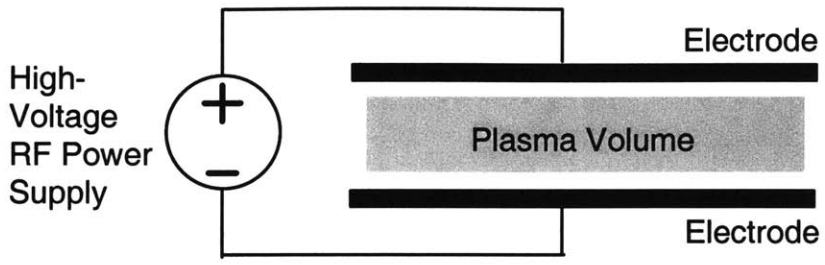

Figure 1: Basic Setup Used to Generate OAUGDP

To generate a weakly-ionized plasma between the electrodes shown in Figure 1, a high voltage is applied across the air gap. Applied current continuously moves electrons to the electrode surface where the high voltages pull electrons into the gap and accelerate these free electrons to ionization energies. It has been observed that these electrons acquire the minimum energy required for ionization of 81 eV [17]. This reduces the power required for plasma generation. Then, via impact ionization, the energretic electrons strip electrons from the surrounding air molecules producing a large supply of positively-charged ions to mix with the free electrons.

This mixture of both positively and negatively charged ions in the same region represents a weakly-ionized gas. The ions and electrons feel an electromagnetic force due to the applied electric between the electrodes. This force is the Lorentz force and is described in Equation 2 [18], and applies to both ions and electrons. The direction of the force depends on the sign of the charge, q.

$$F = ma = -qE - m\nu_c v \tag{2}$$

In Equation 2, the first term on the right hand side describes a retarding force whereby particle momentum is being lost due to collisions. It depends on the collision frequency ν_c, which is larger for electrons that for ions. However, due to the much larger

mass differential between the two particles, ions will lose more momentum per collision and wind up traveling slower than the electrons inside the plasma.

By oscillating the electric field present between the electrodes, it is possible to spatially oscillate the ions and electrons. Using such a scheme, the difference in mobility between the particles can now be taken advantage of. Because the ions move more slowly than the electrons, it will be possible to switch the electric field back and forth at certain frequencies and trap ions between the electrodes without trapping the electrons. This is the "charge-trapping" method.

By trapping ions in a given volume and continually pumping free electrons into the same space, a quasi-steady state is achieved. This weakly-ionized mixture is referred to as a uniform glow-discharge plasma, and exhibits properties to that effect [19]. The frequency of field oscillations necessary to trap ions can be determined from Equation 2 by first making a few more assumptions. The derivation of the critical frequency follows one done by Roth [17].

First, we assume that the applied field is constant across the air gap and equals zero in the other two directions, so that we can write the electric field as in Equation 3.

$$\vec{E} = E_0 \sin(\omega t)\hat{x} \tag{3}$$

Equation 3 can then be substituted into Equation 1 and we can rewrite this as a function of x to obtain Equation 4.

$$m\frac{d^2x}{dt^2} + mv_c\frac{dx}{dt} = eE_0 \sin(\omega t) \tag{4}$$

The general solution to this ordinary differential equation is of the form of Equation 5.

$$x(t) = C_1 \sin(\omega t) + C_2 \cos(\omega t) \tag{5}$$

Using the knowledge that the collision frequency for electrons is much higher than for ions, we can eliminate one of the constants in Equation 5 to obtain the time-dependent position of one of the charged particles between the plates. This is given in Equation 6.

$$x(t) = -\frac{eE_0}{m\omega\nu_c}\cos(\omega t) \tag{6}$$

Then, converting the frequency from radians per second to cycles per second, and substituting the maximum value of the electric field for a parallel-plate configuration [18], we can derive the rms displacement of a charged particle. This is shown in Equation 7.

$$x_{RMS} \approx \frac{eV_{RMS}}{2\pi m\nu_0\nu_c d^2} \tag{7}$$

To satisfy the charge-trapping method, we require this rms displacement to be within the volume between the plates. So, we must satisy Equation 8.

$$x_{RMS} \leq \frac{d}{2} \tag{8}$$

When Equation 8 is satisfied, Equation 7 can be used to place a critical limit on the frequency for charge buildup to occur between the plates. This critical frequency is given in Equation 9.

$$\nu_0 \approx \frac{eV_{RMS}}{\pi m\nu_c d^2} \tag{9}$$

Using Equation 9 with applied voltage values around 5 kV, with an air gap of about 2 cm, and an ion collision frequency around of about 7×10^9 1/s produces a critical plasma generation frequency of about 2 kHz.

2.2 OAUGDP Over a Surface

It is also possible to create an OAUGDP over a surface rather than between two electrodes [20]. This is beneficial for our problem because we are attempting to reduce the impedance mismatch between actuator and fluid inside the cavity. By generating the plasma over a surface, we remove the electrode between the plasma and fluid, providing direct contact between the two.

The reflection coefficient at the fluid-actuator boundary now is of the form of Equation 10, which is derived for two adjoining fluids [10].

$$\frac{\rho_1 c_1}{\rho_2 c_2} = \frac{1+R}{1-R} \tag{10}$$

Density and speed of sound measurements for a weakly-ionized air-based plasma are nearly identical to neutral atmospheric air since both are composed of the same constituents. In fact, since only a small fraction of air molecules are actually ionized in the OAUGDP, it is mostly neutral air. The identical impedances means that Equation 10 can be reduced and the resulting Equation 11 is produced.

$$1 \approx \frac{1+R}{1-R} \Rightarrow (1-R) \approx (1+R) \Rightarrow R \approx 0 \tag{11}$$

As is shown in Equation 11, R goes to zero as the impedances converge, implying no reflection at the boundary between the two fluids. This means that generating the plasma over a surface instead of between two electrodes takes care of the impedance mismatch problem between control surface and fluid.

The procedure for generating an OAUGDP over a surface is much the same as for the two-electrode case. The main difference is that instead of using a large air gap to insulate the electrodes, a smaller volume of high-dielectric material is used. Any good

insulator can be used, and an easy choice for us will be the composite FR5, which most PC boards are made of. This means that a standard PC board can be etched in such a way that the electrodes will remain on either side of the dielectric, and an OAUGDP can be generated over the surface of the PC board.

2.3 Construction of a plasma panel

A panel capable of generating an OAUGDP over its surface was constructed using the method described previously. A PC board was etched so that an electrode grid was present over one surface. A photograph of this panel is shown in Figure 2.

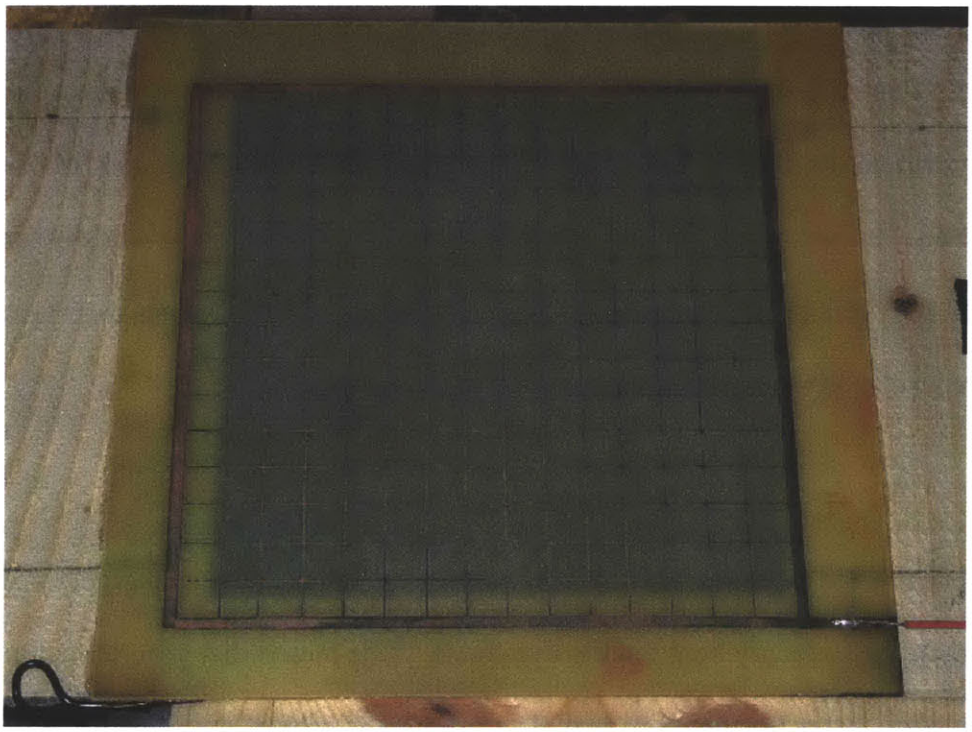

Figure 2: Constructed OAUGDP Panel

A cross-section of the panel is shown in Figure 3 which more clearly illustrates the electrode setup and where the plasma is generated. The top electrode is composed of

a grid with 5mm between grid lines. The bottom electrode is square of 100 square mm area. The electrode design is based on one used by Roth for an OAUGDP panel [21].

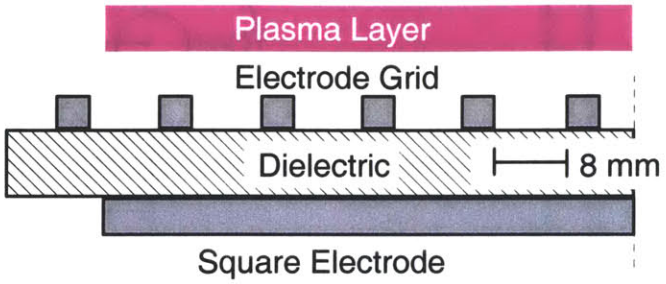

Figure 3: Cross-Section of OAUGDP Panel

With the panel put together, a means for providing a high-voltage RF signal across the electrodes was required. Due to the oscillating nature of the required signal, a simple solution to this was to use an inductor in the form of a standard ignition coil. Such coils are often used to supply high voltages for automotive applications. The inductor follows the law given by Equation 12 [22]. Equation 12 shows that an alternating current would then be able to produce high RF voltages at the coil output.

$$v_L(t) = L\frac{di}{dt} \tag{12}$$

To provide the high-current alternating signal to the coil, a 2N3055 power transistor was used in a current source configuration. A small voltage signal applied to the gate of the transistor would switch the high current on and off to the coil. The circuit designed and constructed to drive the OAUGDP is shown in Figure 4. With inductor values of L = 4H, and a DC power supply capable of providing 8 A, an RF signal with maximum voltage of about 10 kV was possible.

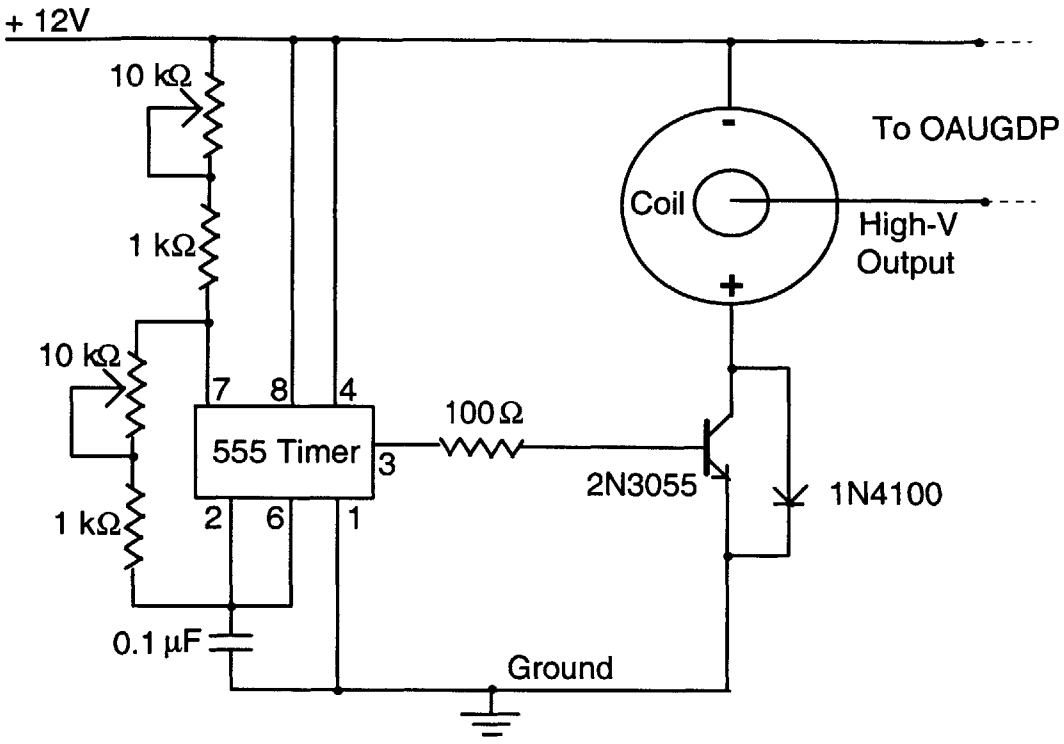

Figure 4: OAUGDP Panel High-Voltage RF Power Supply

The 10k potentiometers are included in the circuit to allow adjustment of the RF frequency of the output voltage. The diode across the power transistor prolongs the transistor life by reducing voltage back across when the coil switches. The high-voltage output line from the coil is linked to the electrode grid on the top side of the OAUGDP panel and the +12V line is tied to the bottom electrode.

Using the power supply in Figure 4 with the constructed panel pictured in Figure 2, it was possible to produce a thin, uniform layer of plasma over the electrode grid. This was verified visually as a purple-blue glow over the panel. A tone was also audible at the plasma generation frequency indicating that the plasma was indeed transferring energy to the surrounding air. A photograph of the panel in operation is shown in Figure 5.

In Figure 5, the plasma layer over the surface can be seen as the light-gray region in the same basic shape as the mesh. The plasma was seen to extend over the area

between the electrodes, and closer visual inspection indicated that plasma covered a good deal of space between the electrodes even though it was not as bright. Active control of the acoustic behavior of the plasma layer was investigated next.

Figure 5: The OAUGDP Panel in Operation

Chapter 3

TONE CANCELLATION EXPERIMENT

3.1 Experimental Setup

A tone cancellation experiment was performed as an initial test on the ability of the OAUGDP to have an effect on the acoustics of a system. The experiment was designed in such a way that acoustic reflections from a surface could be controlled using ANC methods. Tonal cancellation tests are relatively easy to construct and perform and are often used to verify that an ANC system is set up properly. The results from this experiment were intended to be used as a baseline for further experimentation and provide some idea of acoustic reductions that could be expected.

The experiment setup is shown in Figure 6. It consists of two waveguides, designated W_1 and W_2, joined at a right angle with an OAUGDP panel at the vertex of the two waveguides. Both waveguides have square cross-sections with inner widths of 6 inches and thicknesses of ¾ inches, and each waveguide is 2 feet in length. The plasma panel used was described in the previous section, and had dimensions 6 inches by 9 inches, and was 1/16 inches thick.

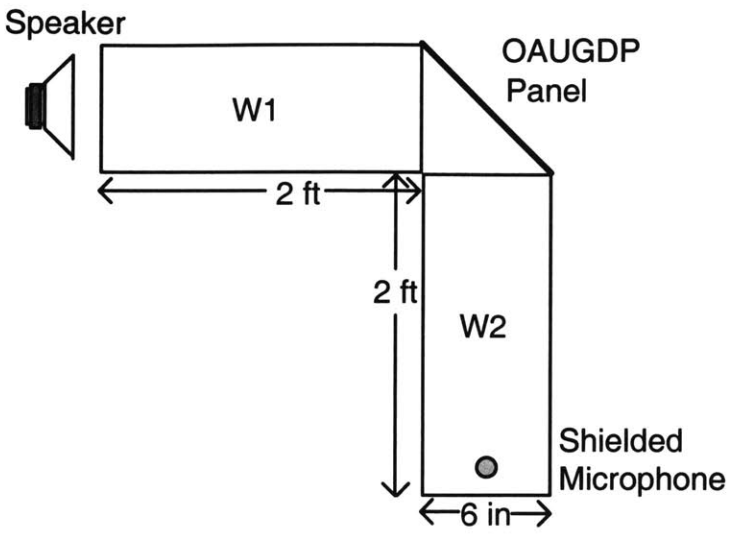

Figure 6: Physical Setup For Tonal Cancellation Experiment

An acoustic test of the system was performed to ensure that reflections from the panel were observable and fit wave models of the system. The desired response from the system was for waves to enter at W_1, reflect off of the plasma panel, and travel down W_2 without loss at the plasma panel. This would mean that to an observer at the output of W_2 with respect to input at W_1, the system's response would look the same as that of a single waveguide with length equal to the length of W_2.

A wave-based model of the system was used to compute the natural frequencies expected from the system given the previous assumptions. This model was compared to experimental data to validate the physical setup. For a waveguide of length 2 feet with two open ends, the natural frequencies of the system are determined from Equation 13 [23]. The speed of sound in Equation 13, c_W, was taken to be 343 meters / second. The variable n denotes the order of the frequency.

$$\nu_n = n\left(\frac{c_W}{2L}\right) \tag{13}$$

Experimental verification of the system's natural frequencies was performed by placing a speaker at the input of W_1 and a microphone at the output of W_2. The speaker was driven by a 1 kHz baseband white noise signal provided by a TekBox. The transfer function from this disturbance to the signal at the microphone was taken, and is shown in Figure 7.

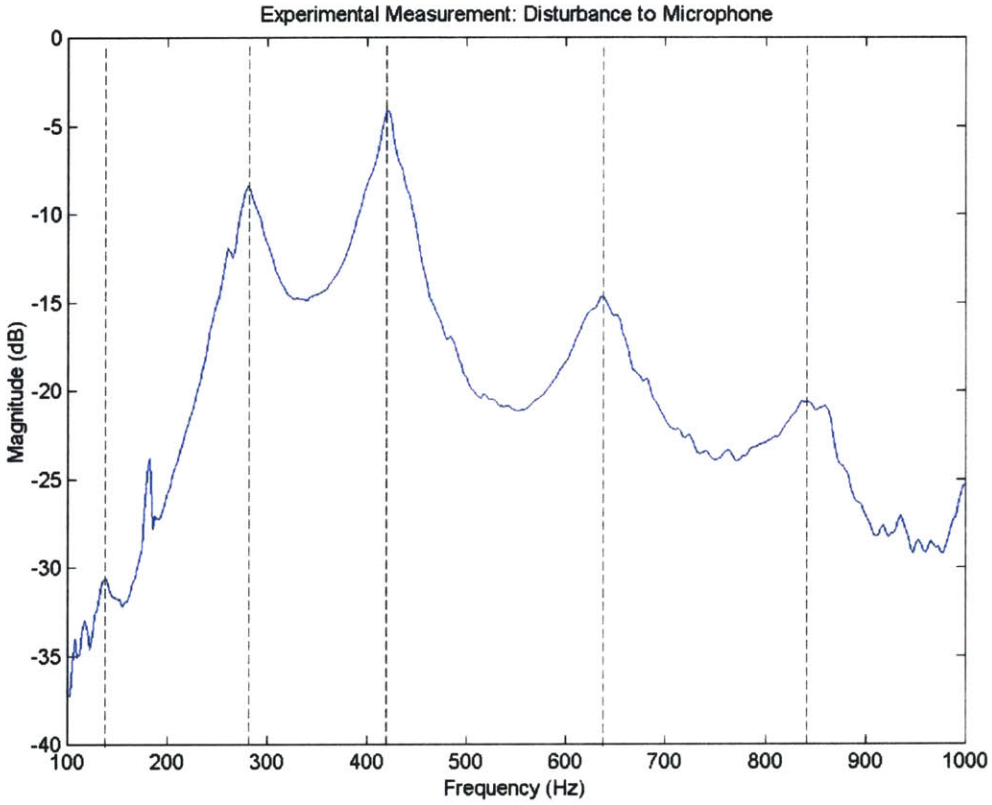

Figure 7: Transfer Function From Disturbance to Microphone

The natural frequencies are seen in Figure 7 as the poles of this transfer function, and are tabulated in Table 1 along with the predicted frequencies from Equation 13 for a 4 foot long waveguide. Table 1 shows very good correlation between experimental and theoretical frequencies, indicating that the assumptions made during the modeling process were valid. The 4^{th} measured acoustic mode is located exactly between the 4^{th}

and 5th predicted acoustic modes, and represents a coupling between those two modes in the experiment.

Table 1: Theoretical and Experimentally Measured Natural Frequencies

Theoretical	Experimental
141 Hz	140 Hz
282 Hz	280 Hz
422 Hz	420 Hz
563 Hz	635 Hz
703 Hz	
844 Hz	843 Hz

Along with the verification from the model, the transfer function in Figure 7 from disturbance to microphone shows that several natural frequencies of the system lie within the control bandwidth of the plasma panel. This bandwidth was previously defined as $\nu_{control} < 500$ Hz for this specific plasma panel. This will allow us to use the same physical setup when attempting to control a specific natural frequency via LQG methods.

The hardware used for the tone cancellation experiment also consisted of a real-time computer which supplied the control signals, and a TekBox which recorded measurements.

3.2 Electro-magnetic Shielding

As mentioned in previous sections, one side effect of the generation of the OAUGDP is the production of electro-magnetic interference at radio frequencies. This interference significantly effects all sensing devices around the waveguides including microphones. To counter this interference, electro-magnetic shielding techniques were used. Because the interference is produced at the long wavelengths associated with radio

waves, shielding can easily be accomplished using faraday cages constructed from metal foils or meshes [24].

Shielded microphones were constructed by using shielded two-conductor cables for connections and by covering the external microphone connections with aluminum foil and copper mesh. A picture of a shielded microphone is shown in Figure 8. The foil and mesh coverings were electrically connected to the shielding of the cable and all tied to ground. These practices reduced external electro-magnetic interference on the microphone signals by over 60 dB, effectively removing it from consideration. Thus, the shielded microphones were assumed to be unaffected by the electro-magnetic interference created in the plasma generation process.

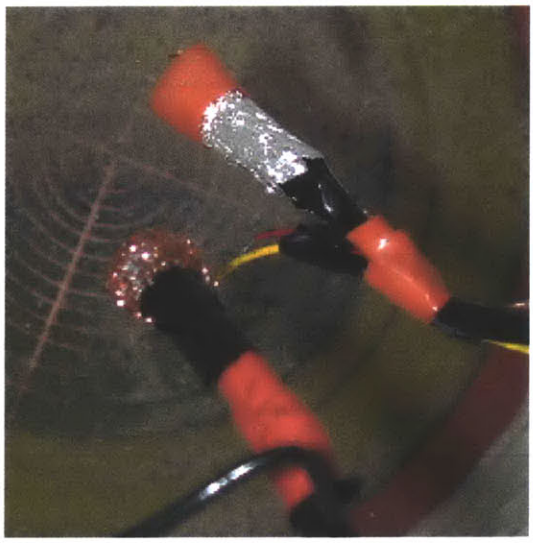

Figure 8: Photograph of a Shielded Microphone and Cable

3.3 Control Method

The method of control for tonal cancellation was to supply a signal to the actuator, thus producing a pressure wave 180 degrees out of phase with the pressure wave

at that point due to the disturbance. A diagram of the control setup is given in Figure 9, and shows how the real-time computer connects to the system.

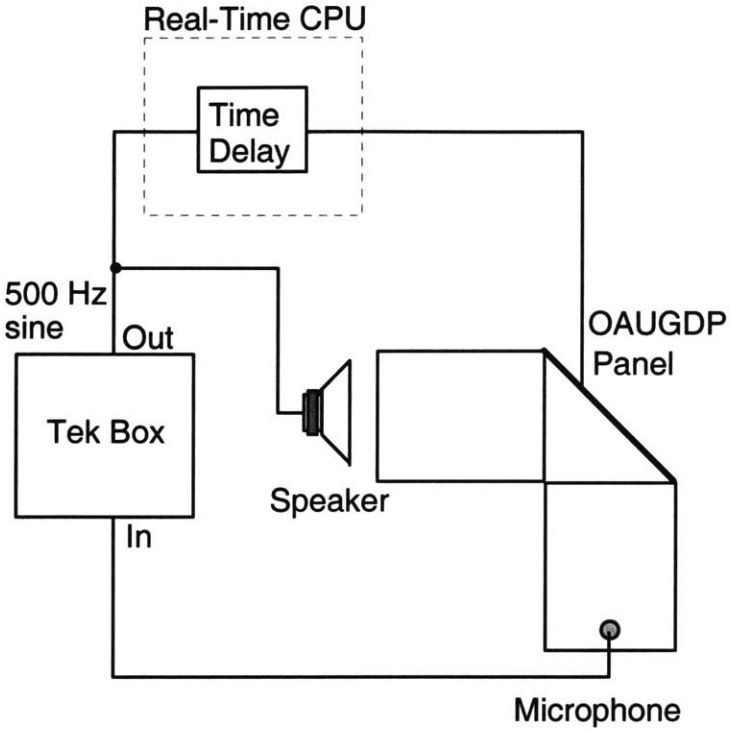

Figure 9: Diagram of the Tone Cancellation Control Method

For the experiment a 500 Hz sine wave was sent to both the disturbance speaker and the plasma panel. A time delay, Δt, was added to the plasma panel line to shift that signal out of phase with the disturbance. The speed of sound, c_W, and the geometry of the system were used to determine the necessary time delay used by the real-time computer in Equation 14. For this experiment, Δt was calculated to be 1.8×10^{-3} seconds.

$$\Delta t = \frac{1}{2}\frac{L}{c_W} \tag{14}$$

3.4 Tone Cancellation Results

Results from this experiment indicate an ability to reduce disturbance noise at the microphone location significantly. This reduction can be seen in a plot of the microphone response for both open and closed loop cases which is shown in Figure 10. The jagged appearance of the signals in Figure 10 is due to the discretization of the data by the TekBox.

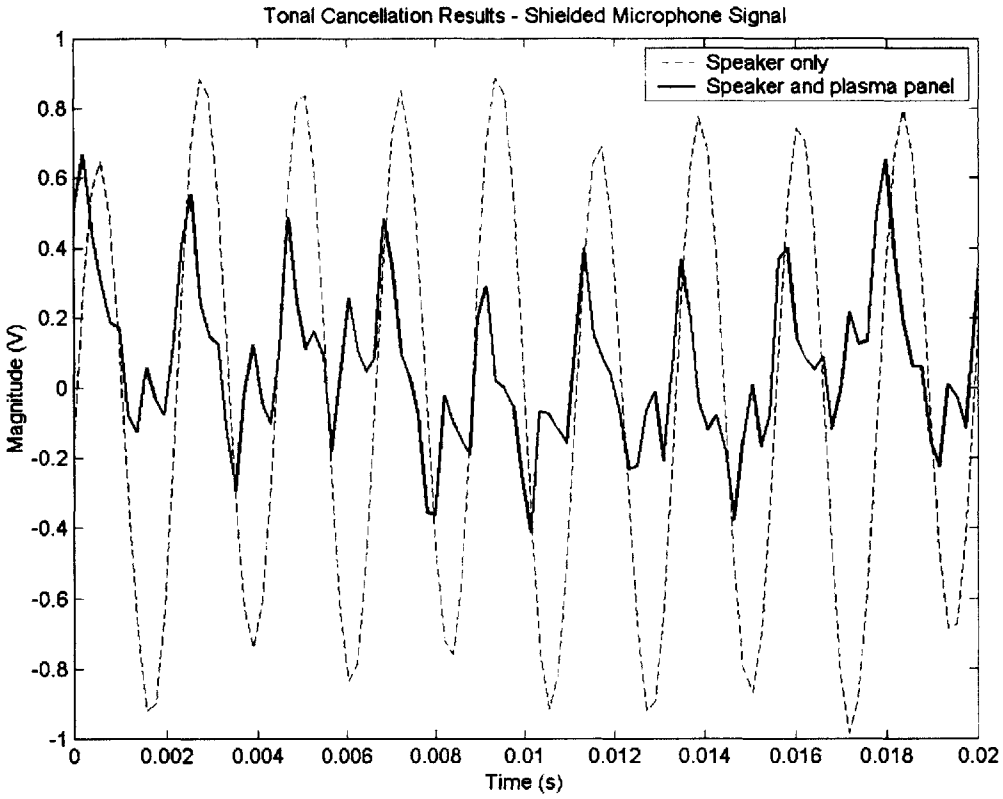

Figure 10: Tone Cancellation Results

Since the disturbance consisted of a single frequency, overall reductions could be determined from the average sound pressure levels of the open and closed loop response. Additionally, since we are really only concerned with relative reductions, no calibration was necessary to convert the microphone signal to a pressure level. The overall reductions are calculated from Equation 15 [25] using an averaging method where m_{open}

and m_{closed} are the open and closed loop microphone responses respectively. In Equation 15, T is determined as the time band used in the integration process to normalize the integrals.

$$reduction(dB) = 20 \times \log\left(\frac{\frac{1}{T}\int m_{open}{}^{2}}{\frac{1}{T}\int m_{closed}{}^{2}}\right) \tag{15}$$

Calculations indicate that for the tonal cancellation experiment the plasma panel was able to reduce the pressure level at the microphone location by 19.6 dB. This was a significant reduction, and confirmed that the panels were able to effect the acoustic environment around them. These results also indicate that reductions of about 20 dB could possibly be realized in broadband experimentation.

Chapter 4

RANDOM DISTURBANCE ATTENUATION EXPERIMENT

4.1 Background

Designing a controller to reduce a random, multi-frequency disturbance requires a more sophisticated technique than the feedforward control used in the previous section. A Linear Quadratic Gaussian (LQG) controller represents an optimal solution to just such a control problem, and uses full-state feedback via an estimator. Designing such a controller requires a model of the plant to be controlled as well as a model of the noise present in the sensor measurements for the estimator. To design an LQG controller, we must be able to write the equations that model the plant in the state-space form. This assumes that such a plant is linear, and time-invariant (LTI). The full details behind the optimization that results in an LQG controller will not be presented here, but the basics used for this project follow.

4.1.1 Full-state Feedback

A state-space model of the plant to be controlled is the basis behind an LQG controller, and satisfies Equation 16 [26]. In Equation 16, the state of the system is represented by the vector x, the vector y is any measurable variable of the system, and u

is an input vector. The natural frequencies and behavior of the plant are determined from the matrix A, and the matrix D is usually a null matrix which assumes there is no feed-forward in the plant.

$$\begin{aligned} \dot{x} &= Ax + Bu \\ y &= Cx + Du \end{aligned} \tag{16}$$

If we use a linear state feedback law, as shown in Equation 17, the dynamics of the plant can be changed.

$$u = -Kx \tag{17}$$

Using Equation 17, we can write the dynamics of the closed-loop plant as in Equation 18. Because the full-state vector has been used for feedback, the dynamics of the entire system can be altered via the eigenvalues. Equation 18 assumes that there is no feed-forward in the system, so that the D matrix is eliminated.

$$\begin{aligned} \dot{x} &= (A - BK)x \\ y &= Cx \end{aligned} \tag{18}$$

4.1.2 The Linear Quadratic Regulator

The linear quadratic regulator (LQR) utilizes full-state feedback to create an optimal solution for the control gain matrix, K, associated with the linear control law given in Equation 17. A quadratic performance metric is minimized to derive this optimal solution. The quadratic metric, or cost, is shown in Equation 19.

$$J = \int_0^\infty \left[x^T(t)Qx(t) + u^T(t)Ru(t)\right]dt \tag{19}$$

The matrices Q and R in Equation 19 weight the states and the control vectors respectively. To minimize the cost, J, the matrix P must satisfy the matrix Riccati

equation, which is given in Equation 20 [27]. The matrices A and B come from the state-space representation of the system.

$$A^T P + PA - PBR^{-1}B^T P + Q = 0 \tag{20}$$

This leads to a gain matrix, K, which can be used in the linear feedback law already discussed. The gain, K, is determined using Equation 21.

$$K = R^{-1}B^T P \tag{21}$$

The gain, K, that results from Equation 21 is an optimal solution to the problem, and weights the states as designed by the matrices Q and R. Using this gain K, specific states of the plant can be controlled without affecting the remaining states, and limits can be placed on the amount of control signal to be input to the system. These properties of the linear quadratic regulator will be used throughout this section.

4.1.3 Full-state Estimation

The linear quadratic regulator requires full-state feedback, but often, the states of the system are not directly observable. Commonly, the states of the plant are estimated, and it is these state estimates that are fed to the controller to produce the control signal. An optimal state observer, called a Kalman filter, can be designed in much the same way as the linear quadratic regulator. To see this, we first assume that our system model now has plant noise, w, and measurement noise, v, and our system equations are given in Equation 22.

$$\begin{aligned} \dot{x} &= Ax + Bu + w \\ y &= Cx + Du + v \end{aligned} \tag{22}$$

Measurement and plant noise can be weighted in the same way that the states and control signal were weighted for the linear quadratic regulator. For systems where a

lot of measurement noise is expected, v is weighted heavily meaning that the resulting observation will be based more on the plant model than the observation. A quadratic cost is associated with the optimal observer and results in a full-state estimate of the system.

4.1.4 Linear Quadratic Gaussian Control

Linear quadratic gaussian control (LQG) combines the techniques of LQR and the Kalman filter. The product of these two methods is a state-space system that can be connected to the output of a plant and produces a signal that can be fed back into the plant for control purposes. A schematic of the LQG method is shown in Figure 11.

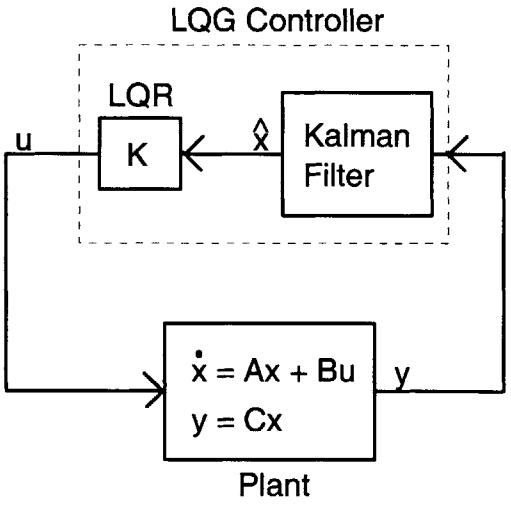

Figure 11: Linear Quadratic Gaussian Controller Setup

4.1.5 Modal Representation

As was mentioned previously, the LQG method for control allows certain states of the system to be controlled, without affecting the remaining states. By transforming the state-space model of the plant into a modal representation, the A matrix reduces to a diagonal matrix consisting of the natural frequencies of the open-loop plant [27]. The Q

matrix will then directly weight certain natural frequencies of the system, allowing the desired frequencies to be targeted for reduction. This will be very useful for us, because it will allow us to target our control at the structural and acoustic natural frequencies that we select.

The modal representation of a state-space system is also known as the diagonal Jordan form of the system. The transformation matrix, T, required to obtain this representation consists of the eigenvectors of the system, which are written as v_1, v_2, ..., v_n in Equation 23.

$$T = [v_1 \quad v_2 \quad \cdots \quad v_n] \tag{23}$$

Using this transformation matrix, the transformed state-space equations are given in Equation 24.

$$\begin{aligned} z &= T^{-1}ATz + T^{-1}Bu \\ y &= CTz + Du \end{aligned} \tag{24}$$

The new matrix describing the dynamics of the system is given by Equation 25, and is a diagonal matrix with the entries being the eigenvalues of the plant.

$$\tilde{A} = T^{-1}AT \tag{25}$$

Using this representation, the quadratic cost function given previously in Equation 19, is now defined for the transformed state z. In this case, the entries of a diagonal Q matrix will directly weight specific eigenvalues of the system. Using this method, specific natural frequencies can be targeted for control, as will be shown in the following sections.

4.2 Random Disturbance Attenuation Experiment

An experiment, using the OAUGDP, was performed in which the disturbance was random. An LQG controller, as described in the previous section was created to target specific frequencies and reduce the acoustic response at a feedback microphone.

4.2.1 Experimental Setup

The same physical setup used for the tonal cancellation experiment was used for this experiment. The only thing that was changed between the two experiments was the control scheme. For the tone cancellation experiment, the disturbance was a known signal of a single frequency, so this information was fed forward to the actuator. For the random disturbance case, the disturbance would contain multiple frequencies, and be unknown to the controller, so feedback methods would be required. A diagram of the control method used for this problem is shown in Figure 12.

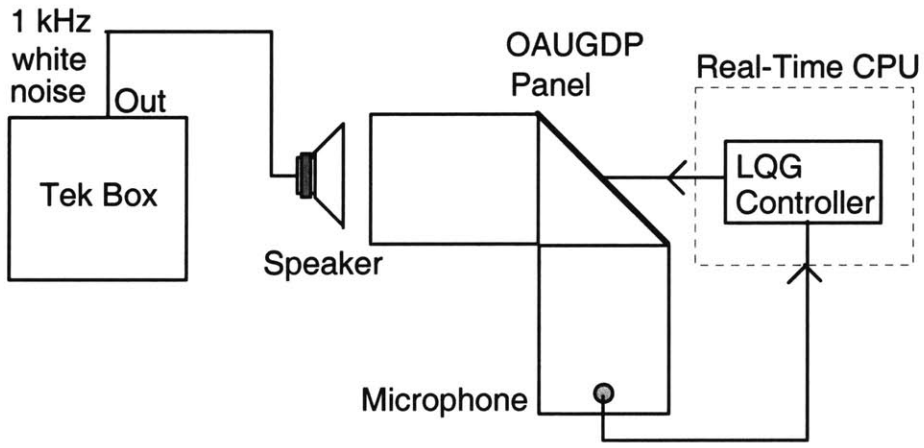

Figure 12: Diagram of the random disturbance control method

4.2.2 Hardware

The hardware used for this experiment consisted of the angled waveguides, an OAUGDP panel as described in Chapter 2, electronics required to drive the panel, a Tek Box capable of taking transfer functions and producing a white-noise disturbance, and a real-time computer for control. A photograph of the waveguide setup is shown in Figure 13. The OAUGDP panel is at the vertex of the waveguides. The left waveguide is covered in metal to shield the speaker and other electronics from interference.

Figure 13: Photograph of the Waveguide Assembly

A shielded microphone was used as the feedback sensor for the LQG controller. The control signal was added via amplitude modulation to a plasma generation signal at 500 Hz by the real-time computer. This total signal was then sent to the high-voltage circuitry and then to the plasma panel.

4.2.3 Experimental Procedure

The entire experimental process began by taking transfer functions from disturbance and control to sensor. While the transfer functions from disturbance, or speaker, to microphone were already obtainable, to obtain the transfer function from control source to microphone required a special method.

To take the transfer function from control to sensor, a white-noise, 1 kHz baseband disturbance was created by the TekBox and sent to the real-time computer. A special program was created that received this signal and added to it the plasma generation signal of 500 Hz. This signal was sent out to the plasma panel, and the transfer function from the 1 kHz white noise to the microphone was taken by the Tek Box. This transfer function necessarily had spikes at 500 Hz and harmonic frequencies due to the addition of the plasma generation signal. A plot of the control source to microphone transfer function is shown in Figure 14.

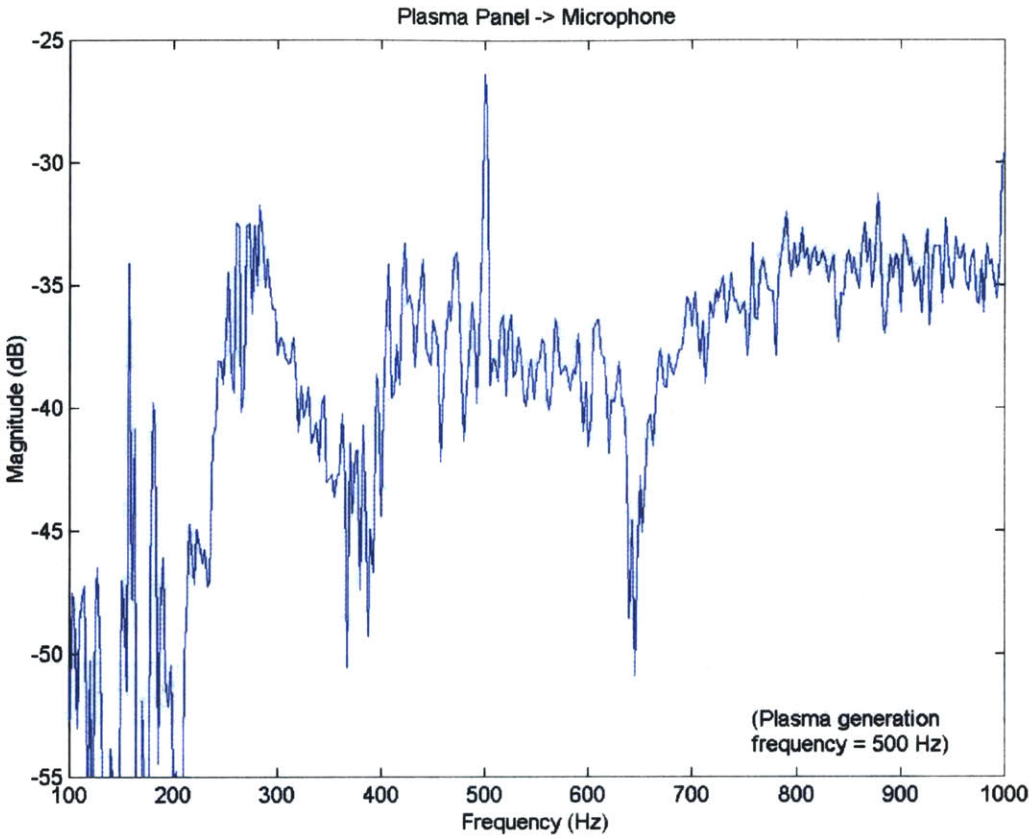

Figure 14: Plasma Panel (Control Source) to Microphone (Sensor)

To complete the experimental process, these two transfer functions were combined into a state-space model of the plant using the FORSE algorithm. This resulted in a 38-state state-space model of the plant. This model was transformed into a modal form using the modal transformation given in the previous chapter. The natural frequencies of the plant were then linked directly to diagonal entries of the Q matrix in LQG control design, and the Q matrix was set to weight specific frequencies. The controller was then designed in MATLAB and a Kalman filter was added as a full-state observer.

This produced a SISO, 38-state regulator with a microphone as the input and the plasma panel as the output. This regulator was downloaded to the real-time computer and white noise was fed to the speaker from the Tek Box. Open and closed loop

measurements from the disturbance to microphone were taken, completing the experiment. A flow diagram of the entire experimental process is given in Figure 15.

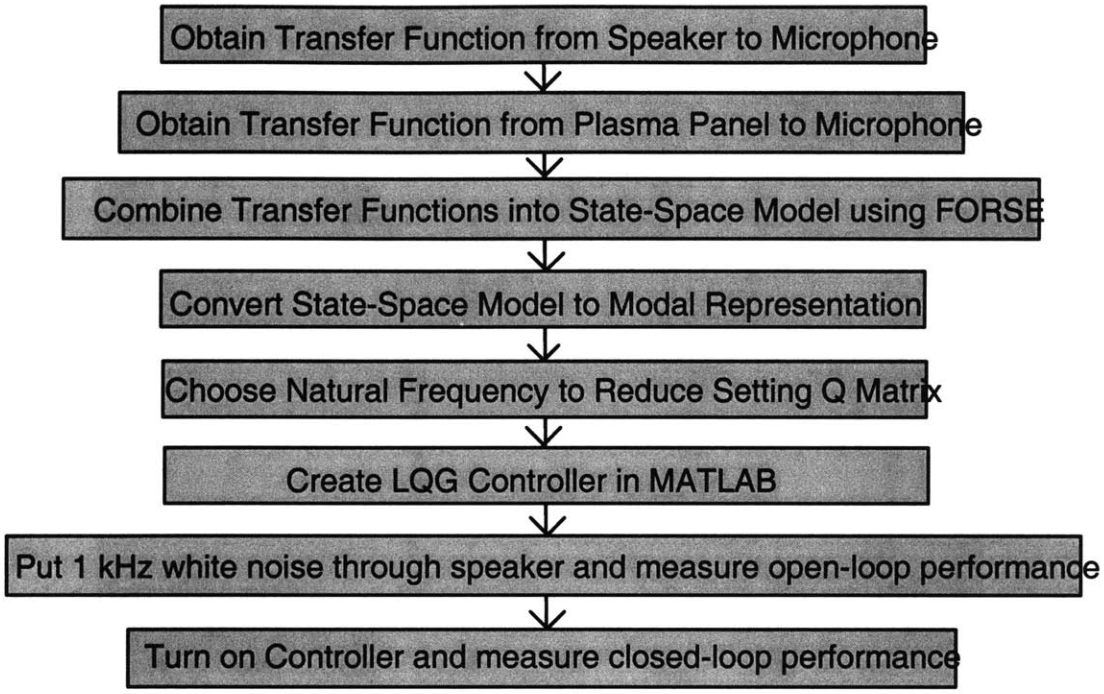

Figure 15: Flow Diagram of the Experimental Procedure

4.3 Results

Results from the random disturbance rejection experiment are given below. The first highly-observable acoustic mode at 280 Hz was selected as the target for the LQG controller. The plasma generation frequency was set at 500 Hz. Open and closed loop transfer functions are compared in Figure 16.

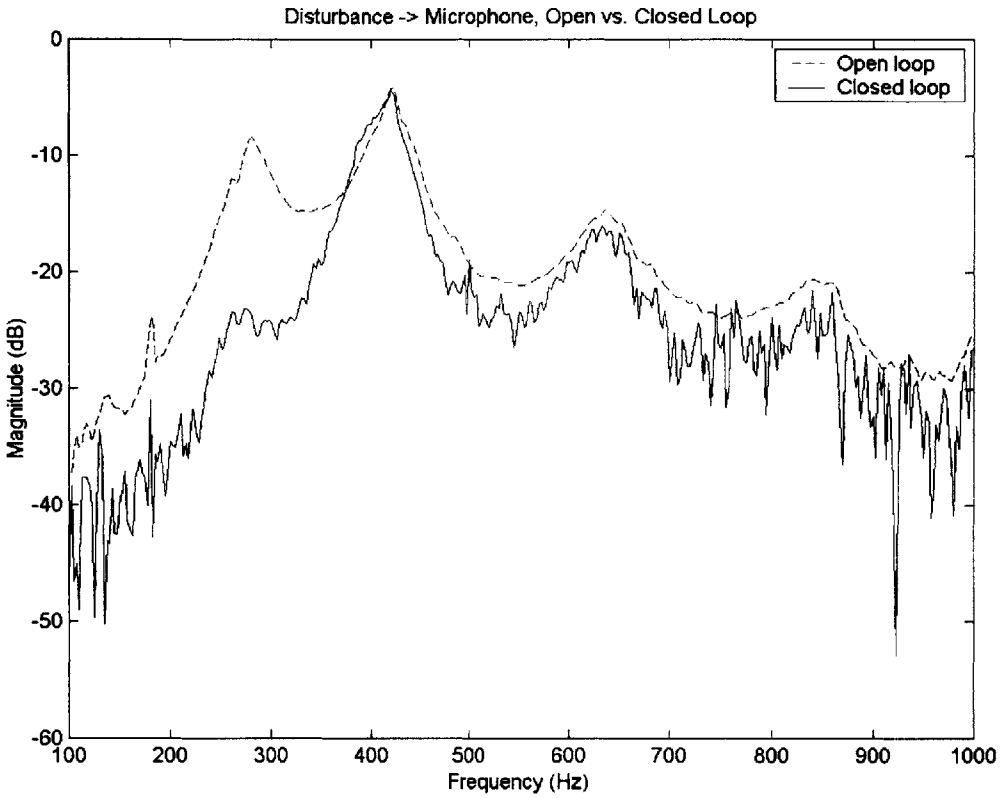

Figure 16: Flow Diagram of the Experimental Procedure

Figure 16 shows a reduction of the sound at the feedback microphone at the first observable acoustic mode. This reduction was calculated more specifically to be 15.4 dB over the 5 Hz frequency range from 277.5 Hz to 282.5 Hz. The broadband reductions were calculated over the frequency range from 122 to 372.5 Hz as 9.7 dB. These attenuations compare well with those that might be expected from the tone cancellation results.

While these reductions are better than previously attained at MIT for acoustic modes, they do not compare directly with those experiments [28]. One reason is that these results are not global attenuations, but rather are local reductions at the feedback

sensor location. Previous work at MIT all involved ASAC methods which are global in nature.

Chapter 5

STRUCTURAL-ACOUSTIC CONTROL

5.1 Motivation

Active structural-acoustic control (ASAC), as described in the previous sections uses structurally-embedded actuators to globally reduce the sound transmitted into a cavity. It does this by de-vibrating the structure at its natural frequencies where transmission is highest. The end goal of the research described here is to combine the OAUGDP work presented previously with ASAC methods to produce a panel capable of both methods of actuation. It was hoped that by combining the two, more significant noise reductions could be achieved.

5.2 Experimental Setup

A new experimental setup was created to allow for incorporation of structural control. The setup physically resembles that used in previous work at MIT. It consists of several cylindrical sections that can be placed on top of each other, allowing a plate to be placed between sections. By placing a speaker at one end of the cylinder, transmission through a plate, as well as reflection at a plate could be observed. A photograph of the assembled cylinder is shown in Figure 16.

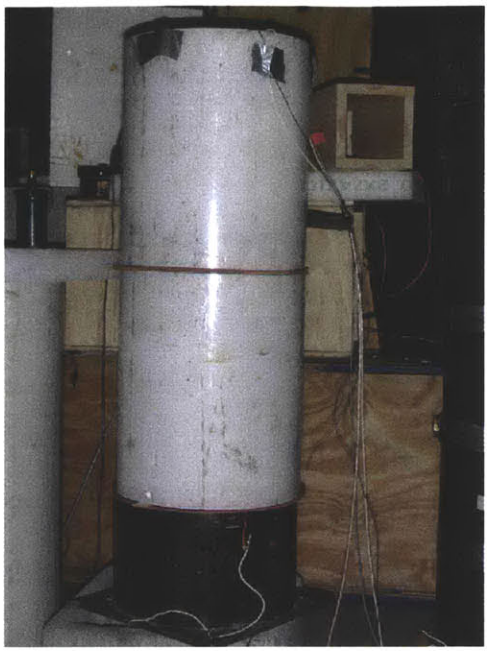

Figure 17: Assembled Acoustic Testbed

The testbed depicted in Figure 17 is 37.5 inches tall when assembled. The speaker rests in the 7.5 inch metallic section at the bottom of the tube, and the plate is located between the two 15 inch white sections. The white sections are PVC pipe, which has an inner radius of 12 inches, and an outer radius of 12.125 inches. PVC was chosen as the material because it is a good insulator and would prevent arcing from the OAUGDP panel to the cylinder.

To provide structural actuation, a plate was constructed and placed inside the PVC testbed. A PC-board panel was used since an OAUGDP has already been demonstrated over the surface of such a panel. The panel was constructed of epoxy with glass fibers, and was 12 inches × 12 inches × 1/16 inches thick. A piezoelectric patch was bonded to the panel at its center. A photograph of the panel is shown in Figure 18.

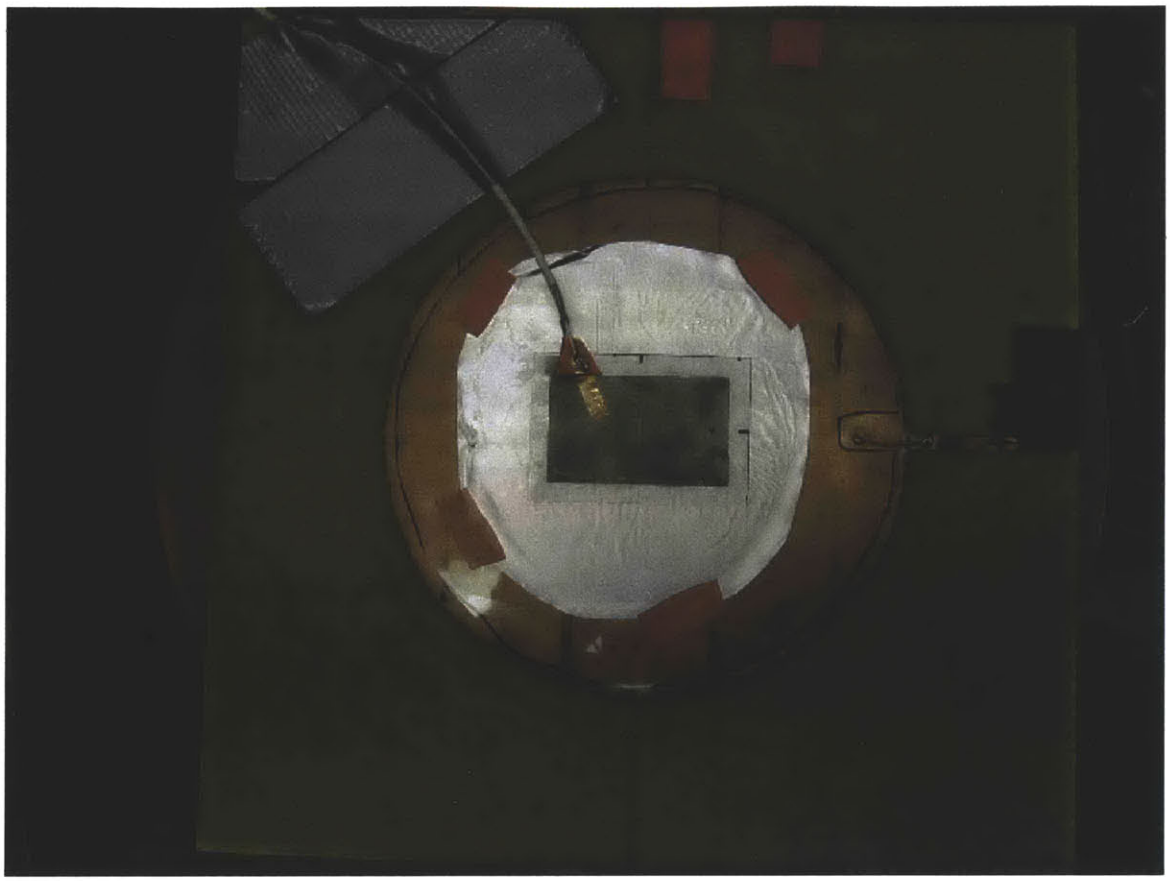

Figure 18: Piezoelectric Element Bonded to Panel

Several things in Figure 18 require further explanation. The large copper circle on the panel was etched onto the panel, and previously covered the entire back side. It had been etched to allow production of an OAUGDP over the panel's surface. This will be discussed in a later section. A two-conductor wire which is seen as the white wire in Figure 18 was connected with one conductor to each side of the PZT patch to produce the actuation signal to the PZT.

The piezoelectric patch, visible in the center of the panel has several layers between it and the copper circle. These layers are there to shield the PZT from interference from the OAUGDP that would eventually be produced on the other side of

the panel. Layers of insulation are also present to maintain a separate ground for the PZT. A more thorough description of the extra layers is shown in Figure 19.

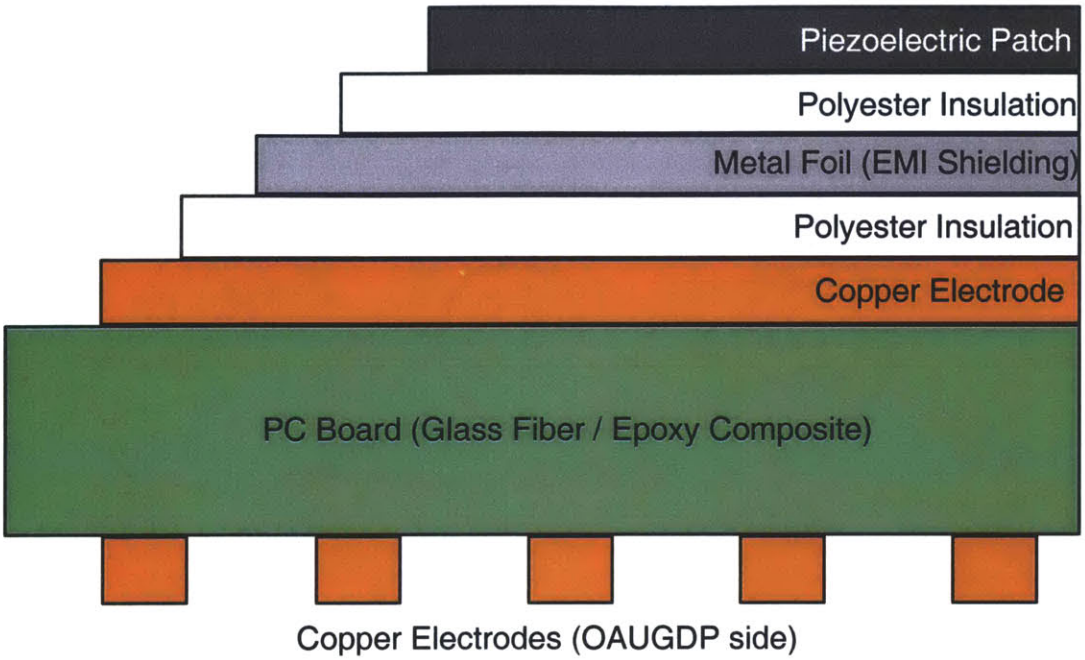

Figure 19: Cross-Section of Layers Applied to Panel

Figure 19 shows the PC board with electrodes on both sides as in previous panels described to generate an OAUGDP over their surfaces. A clear polymer layer insulates the metal foil used to shield the electro-magnetic interference from the electrode. The piezoelectric patch is shielded from the foil layer on the other side by a second polyester layer. All the layers described above were very thin and bonded sequentially to one another to allow for a good structural bond between the PZT and the panel. A good structural bond is required for actuation of the panel.

To complete the EMI shielding process, a foil box was created and bonded to the top of the layers described previously. The foil box only had physical contact with the foil layer under the layers, producing a thin metal enclosure over the entire PZT patch.

The foil box also covered the area where the shielded cable connected to the PZT patch. A picture of the foil box enclosing the PZT is shown in Figure 20.

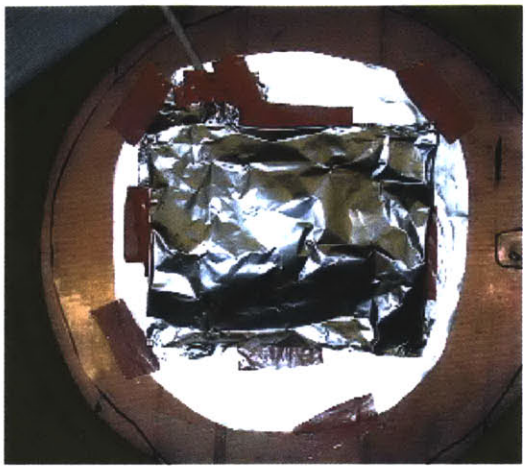

Figure 20: Foil Enclosure for EMI Shielding of PZT

Using the hardware described, it is possible to structurally actuate the constructed panel. However, to actively control the panel, a background in the vibrational response of such a panel is required as well as a brief understanding of how a PZT patch actuates.

5.3 Structural Background

The natural frequencies of a clamped circular plate are determined from the differential equation for forced vibration response of a circular plate. This differential equation is shown in Equation 26 [29].

$$D\nabla^4 w + \rho h\ddot{w} = q(r,t) \tag{26}$$

In Equation 26, ρ is the density of the plate and h is the thickness. The variable D is material dependent and is defined by Equation 27.

$$D = \frac{Eh^3}{12(1-\nu^2)} \tag{27}$$

In Equation 27, E is Young's modulus of elasticity, and ν is the Poisson ratio. For the plate being used, we assume that the layer of copper over the surface is negligible to the vibrational response of the plate, as well as the layers over the center of the plate. The panel is an epoxy resin and glass cloth composite with material properties [30] as E = 15 Gpa, ν = 0.3, ρ = 1.85 g/cc, and as already stated, thickness h = 1/16 inches. These values set D = 5.496.

To determine the natural frequencies, we assume a harmonic solution of the form of Equation 28 [31].

$$W(r,\theta) = \sum_{n=0}^{\infty} W_n(r)(\cos n\theta + \sin n\theta) \tag{28}$$

Substituting this solution into Equation 26, and utilizing Bessel functions, the frequency equation can be written as shown in Equation 29.

$$J_n(\beta a)I_{n+1}(\beta a) + I_n(\beta a)J_{n+1}(\beta a) = 0 \tag{29}$$

The natural frequencies are defined by the roots of this equation, and are computed by Equation 30.

$$\omega_i = \frac{(\beta_i a)^2}{a^2}\sqrt{\frac{D}{\rho h}} \quad rad/s \tag{30}$$

The roots of Equation 29 define the values of $\beta_i a$, and the first three roots of Equation 29 are given in Table 2. These roots define the first three axisymmetric vibration modes of the plate. Since the first mode was of primary interest, it was the target of our controller. Table 2 also lists the first three axisymmetric natural frequencies of the plate in Hz.

Table 2: First Three Axisymmetric Natural Plate Frequencies

I	$\beta_i a$	ω_i (Hz)
0	3.1961	95.8
1	6.3064	372.9
2	9.4395	835.3

A clamped plate also has natural vibration modes that are not axisymmetric. For these modes, the frequency equation has roots $\beta_{ns}a$ where n is now ≥ 0. The first three of these roots all occur for zero nodal circles (s=0). These roots along with the corresponding natural frequencies are given in Table 3.

Table 3: First Three Non-axisymmetric Natural Plate Frequencies

N	$\beta_{n0}a$	ω_n (Hz)
1	4.61	199.3
2	5.91	327.6
3	7.14	478.1

From Tables 2 and 3, we see that the first natural frequency of the plate is approximately 96 Hz. The modeshape at this frequency is plotted in Figure 21. This modeshape shows the largest deflection at the center of the plate, and no nodal lines other than the boundary condition at the plate's edge. The plotted modeshape has been normalized in this case.

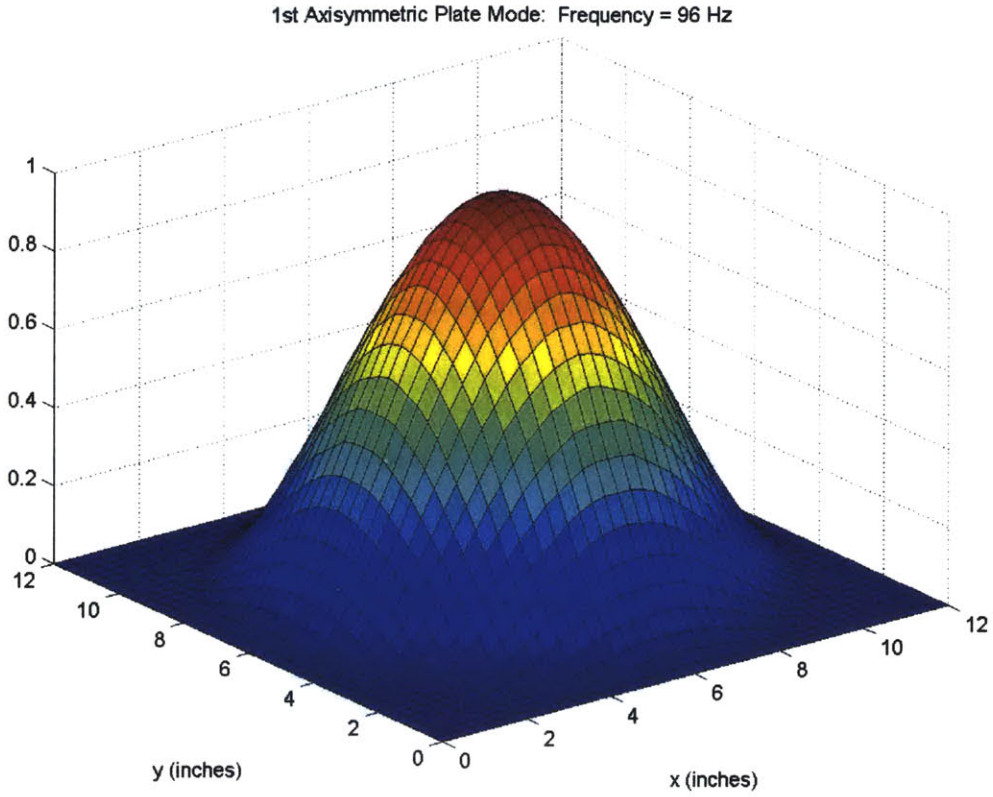

Figure 21: First Natural Plate Modeshape ($\omega = 96$ Hz)

The first two axisymmetric plate modes are easily observable by taking a transfer function of the cylinder acoustic response. To accomplish this, the plate was placed in the acoustic chamber, and the speaker at the chamber bottom was driven with a 1 kHz baseband white noise signal. A microphone was positioned in the cylinder above the plate, and the top of the cylinder was capped. This setup is further illustrated in Figure 22.

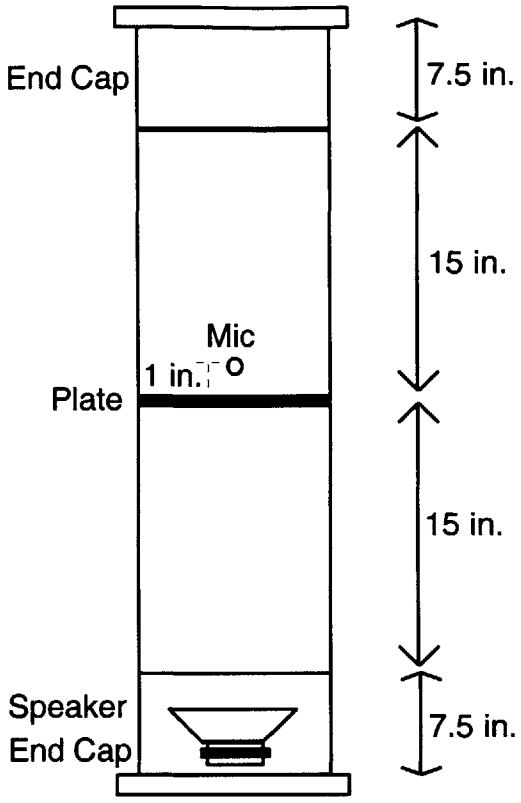

Figure 22: Structural Control Setup

The 1 kHz white noise was supplied by the Tek Box, and the transfer function from this signal to the microphone response was taken. This transfer function is shown in Figure 23 along with the first 3 theoretically determined axisymmetric natural frequencies. Figure 23 shows there is a good correlation between the predicted natural frequencies (dashed lines) and those measured experimentally (solid line peaks). Differences between the two can be attributed to imperfections in the plate and boundary conditions that might alter the material or geometric properties of the setup.

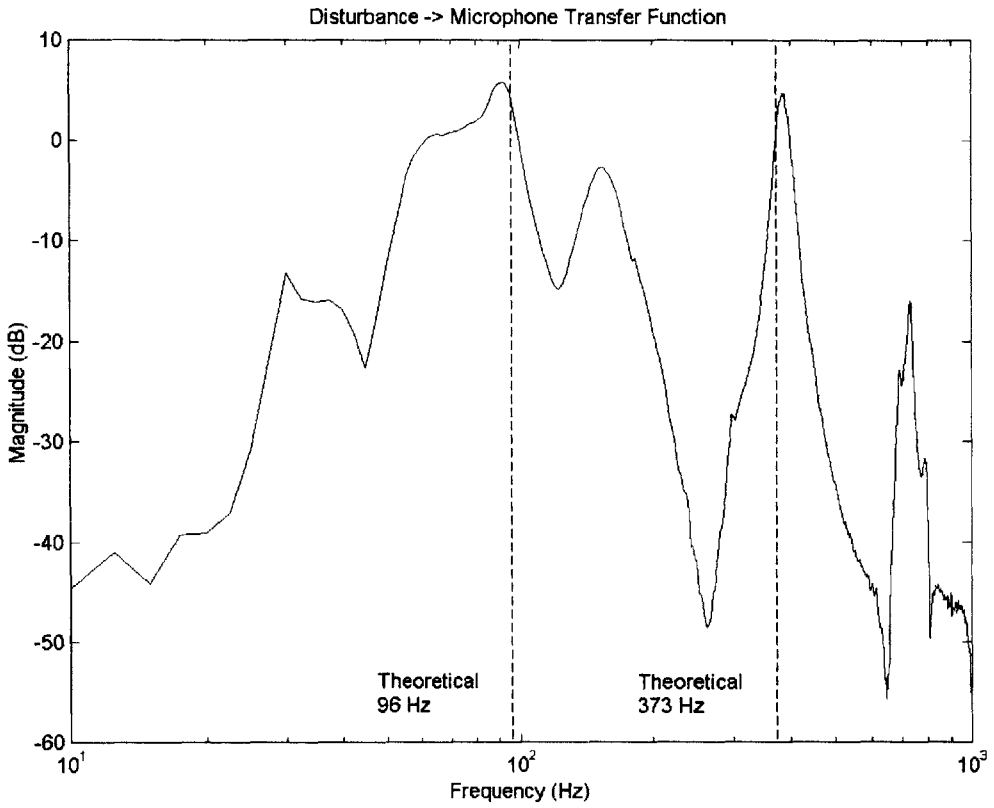

Figure 23: Experimental and Theoretical Plate Natural Frequencies

The non-axisymmetric modes are not as significant, and combine with the acoustic modes to produce some of the other poles observable in Figure 23. But, knowing that the first structural mode occurs around 90 Hz enables us to target it in LQG control, so we have all the structural background necessary to accomplish this.

5.4 Piezoelectric Background

Piezoelectric materials utilize molecular locations to transfer electrical displacement into mechanical stress and vice-versa. The constitutive equations that describe this process are shown in Equation 31 [32].

$$D_i = \varepsilon^s{}_{ik} E_k + e_{ikl} S_{kl}$$
$$T_{ij} = -e_{kij} E_k + c^E{}_{ijkl} S_{kl} \tag{31}$$

The matrices ε^S and c^E in Equation 31 are material dependent and are referred to as the dielectric and stiffness matrices. The e matrix describes the coupling between the electric displacement and material stress. Equation 31 shows that by applying an electric displacement inside a piezoelectric material, we can affect a mechanical stress. If the piezoelectric patch is bonded to a structure, the lumped-mass representation of the structure can be modified to include the equations in Equation 31, and fully describe the response to an applied electric displacement.

Since measurement models are being used for this work, a fully coupled piezoelectric-structural model of a patch bonded to a plate is not required. A more detailed explanation of the subject can be found in the paper by Hagood [33].

5.4 Structural Control Results

Structural control was produced in the same way as described in previous sections. LQG techniques were used, allowing specific natural frequencies of the system to be targeted. In this case, the first mode of the plate was targeted for reduction. Instead of using a structural sensor for feedback to the controller, a microphone was used. This microphone was collocated with the piezoelectric patch, and positioned close to the plate to ensure that it senses the pressure response due to plate vibration. The setup is the same as that shown in Figure 22.

As Figure 22 shows, the microphone was located approximately 1 inch above the plate. Both ends of the PVC tube were capped with metal cylindrical sections for two reasons. First, so that reflections could also be observed in the tube section with the

microphone. This more closely models the interior of a payload fairing in which reflections at the other end of the cavity play a role in the interior acoustic response. Second, the end caps used were very heavy solid metal sections that provided the weight necessary to produce a clamped boundary condition on the plate.

Open loop transfer functions from the disturbance and control source to the microphone were taken and are shown in Figure 24.

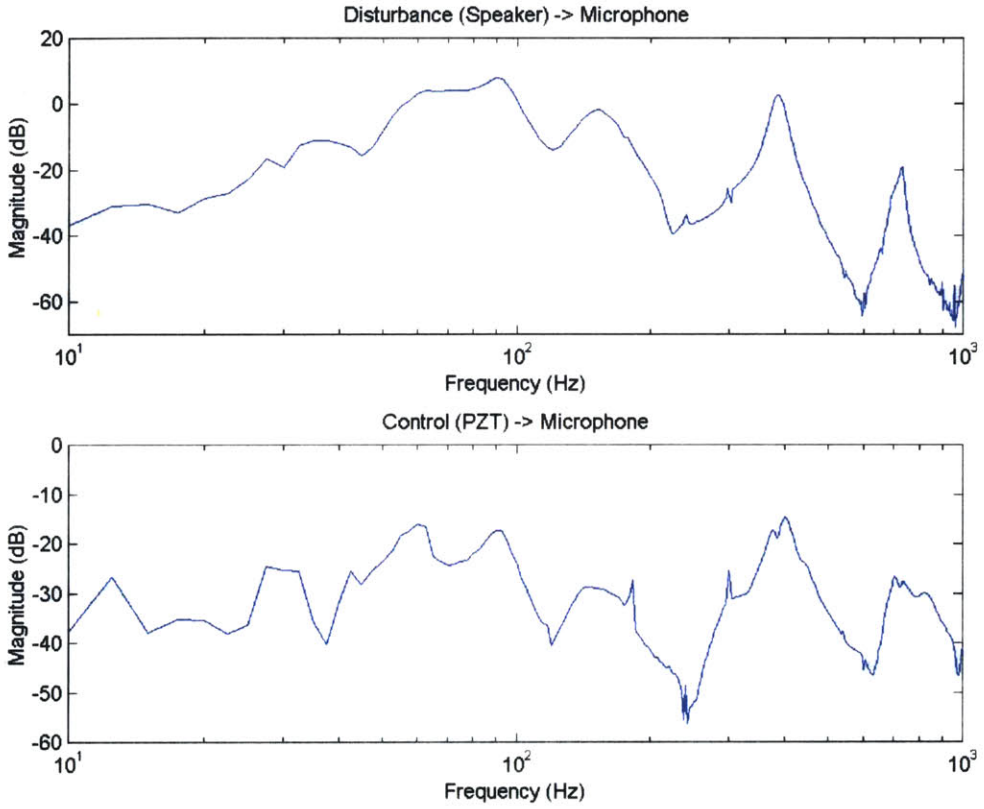

Figure 24: Disturbance and Control Source to Microphone

These transfer functions were used to design an LQG controller targeting the first structural mode at 90 Hz. This controller was applied, and open and closed loop transfer functions are given in Figure 25. The experiment resulted in reductions at the first structural mode of 8.3 dB.

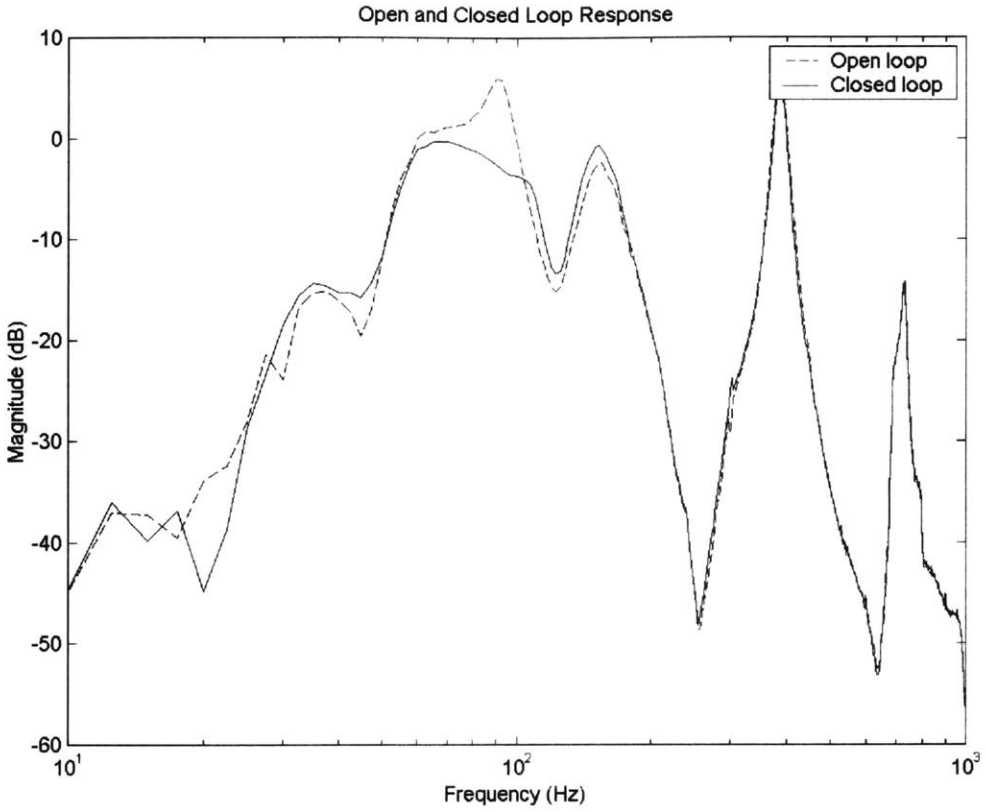

Figure 25: Open vs. Closed Loop – Structural Control

Chapter 6

COMBINED STRUCTURAL AND OAUGDP CONTROL

6.1 Setup

A modal version of the OAUGDP was developed which was hoped to produce global reductions of a similar magnitude to those presented in Chapter 4. This section details an experiment designed to combine the structural-acoustic methods presented before with the modal OAUGDP actuator. The hope of this experiment was that both techniques could be combined to create larger noise reductions than could be obtained by either of the methods separately. To complete this experiment, an active panel with structural and OAUGDP elements was constructed.

The panel used for this experiment was the same one used previously for structural control, but with modifications made to the side opposite the one with the piezoelectric patch. To allow plasma generation over the panel's second surface, an electrode grid was required. This grid was etched chemically, and a photograph of the etched grid is shown in Figure 26.

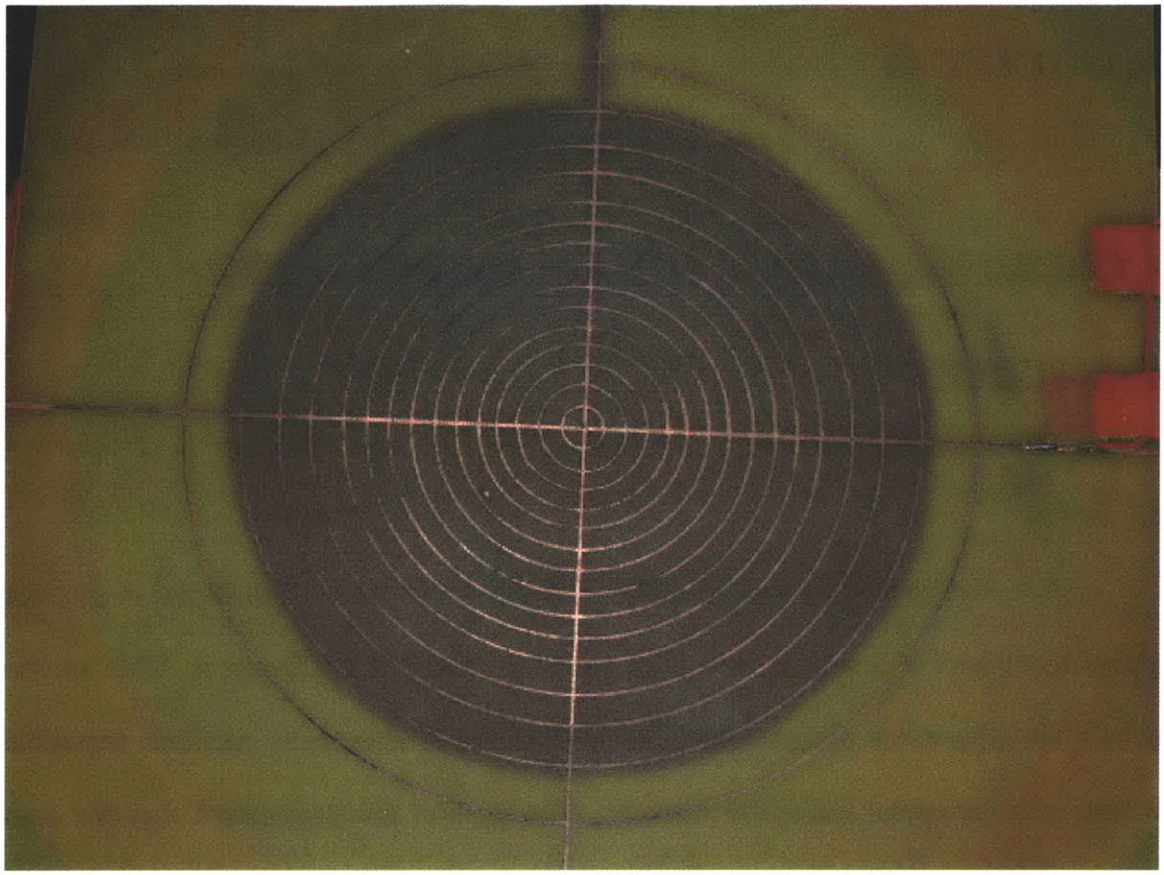

Figure 26: OAUGDP Electrode Grid

The specific pattern of the grid shown in Figure 25 was an attempt to solve one of the defects associated with ANC. As it has been stated previously, ANC methods often do not result in global sound reductions. That is, noise is only attenuated at the location of the feedback sensor, unless there is an accurate, global model of the system dynamics. If we could take into account the modal response of the system, and could shape our acoustic actuator to deliver a modal control source, we could effect global noise reductions.

The simplest mode for actuation in this case is the first structural mode of the plate, and this was selected as the mode to be targeted. This modeshape is already known

and was shown previously in Figure 20. By tailoring the plasma generation grid to this shape, we hoped to globally actuate on this mode.

A modal actuator was designed by integrating the area under the modeshape. This integrated function was divided into several areas of the same size, and integer numbers of electrode rings allotted to each area based on size. For the first structural mode, this meant less space between rings near the center and more space at the edges. The spacing between electrode rings was calculated from the integrated modeshape and is shown in Figure 27.

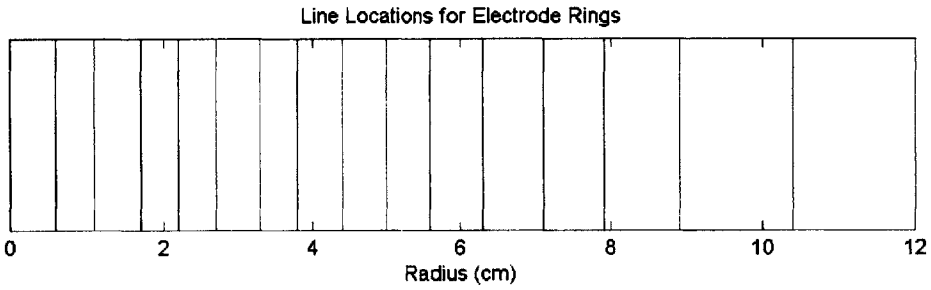

Figure 27: Electrode Ring Locations vs. Radius

Figure 27 shows the first electrode ring at 6 mm from the plate center and the last ring at 10.4 cm from the center. Symmetric rings were used due to the axisymmetric nature of the first plate mode. The location of the rings is such that the amount of plasma generated over the surface of the plate would be proportional to the first modeshape.

The active panel used for this experiment consisted, then, of an OAUGDP generating grid on one side and a structural actuator on the other. The idea behind the panel was to face the OAUGDP side of the panel into the cavity and use it to control interior noise while the structural actuator would control transmission from an external source. A schematic of this is shown in Figure 28.

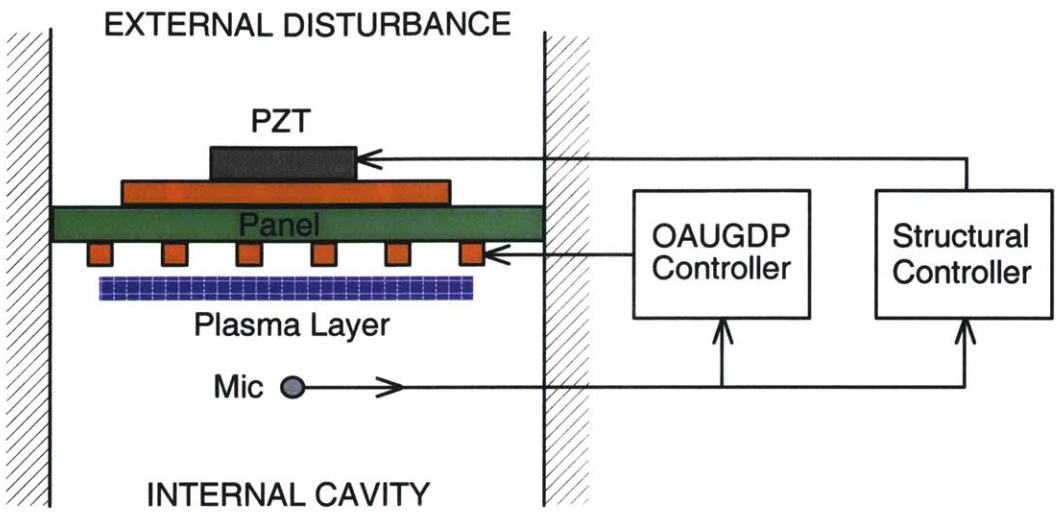

Figure 28: Schematic for Combined Control Experiment

The physical setup for this experiment was the same as that for the structural control experiment. The PVC tube with capped ends was used, with the speaker and panel in the same location as described in Figure 22.

The LQG techniques used previously were also used for the combined control experiment. Two controllers were designed separately and then run concurrently for this experiment. Both controllers used the same microphone for feedback, although a performance microphone was used at times to determine the global effectiveness of the control.

6.2 Combined Control Results

A few variations were performed of the combined control experiment. In the first case, the two controllers were set to target different system modes. The structural controller was designed to target the first structural mode at 90 Hz, and the OAUGDP controller was designed to reduce the second structural mode at 373 Hz. The primary motivation behind this experiment was to test whether the two controllers would function

at the same time without interference, and whether the controllers would complement one another.

Both controllers were run separately first, and then together. Open and closed loop results for the structural controller alone and the OAUGDP controller alone are shown in Figure 29 and Figure 30 respectively. The structural controller reduced the 90 Hz mode by 8.2 dB and the OAUGDP controller reduced the 385 Hz mode by 4.5 dB

Figure 31 shows the result of running both controllers at the same time. The attenuations observed for the combined experiment were nearly the same as that for the targeted modes when the controllers were run independently. The reductions of the combined controller were 7.6 dB at 90 Hz and 6.5 dB at 385 Hz.

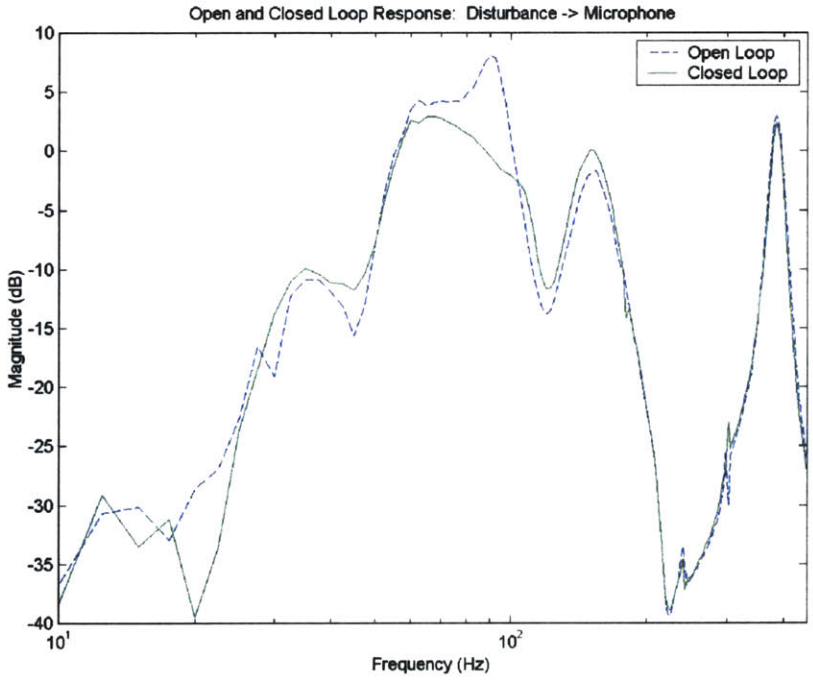

Figure 29: Open and Closed Loop Structural Control at 90 Hz

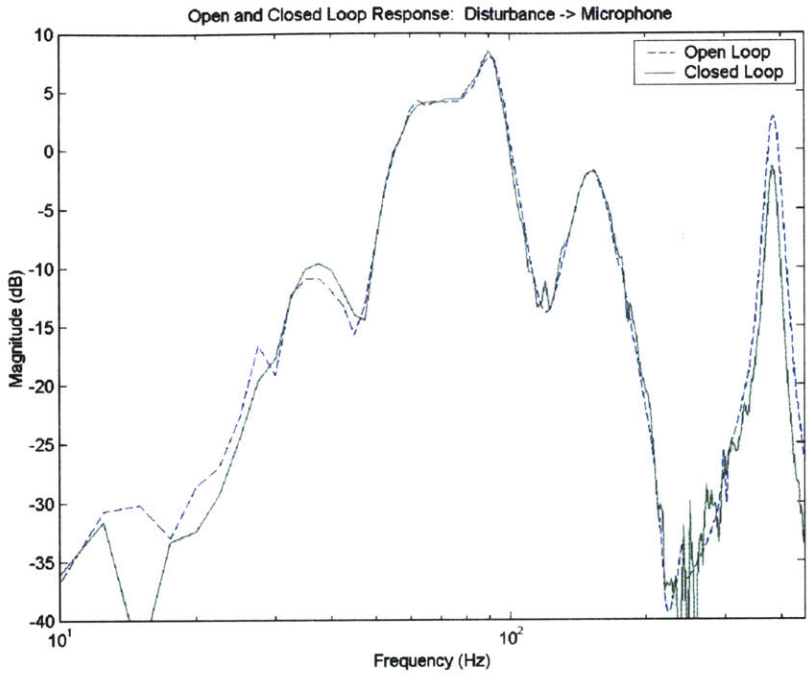

Figure 30: Open and Closed Loop OAUGDP Control at 373 Hz

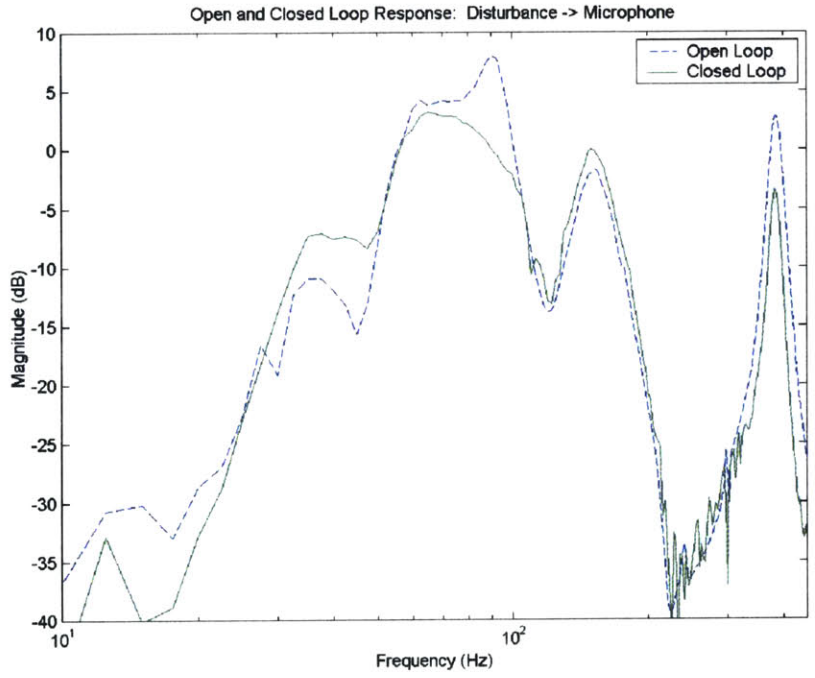

Figure 31: Combined OAUGDP and Structural Control

A table of the results from this experiment is given in Table 4.

Table 4: Combined Structural and OAUGDP Control Reductions

Controller	Frequency	
	90 Hz	385 Hz
Structural Only	8.2 dB	-
OAUGDP Only	-	4.5 dB
Combined	7.6 dB	6.5 dB

Next, both controllers were designed to target the same frequency, the first structural mode at 90 Hz. Open and closed loop results from each controller alone are shown in Figure 32 and Figure 33. Reductions from the structural controller alone were 4.9 dB and from the OAUGDP control alone were 1.3 dB. While the reductions at these specific frequencies were much less than the previous experiment, other frequencies showed reductions on the same order as the previous experiment.

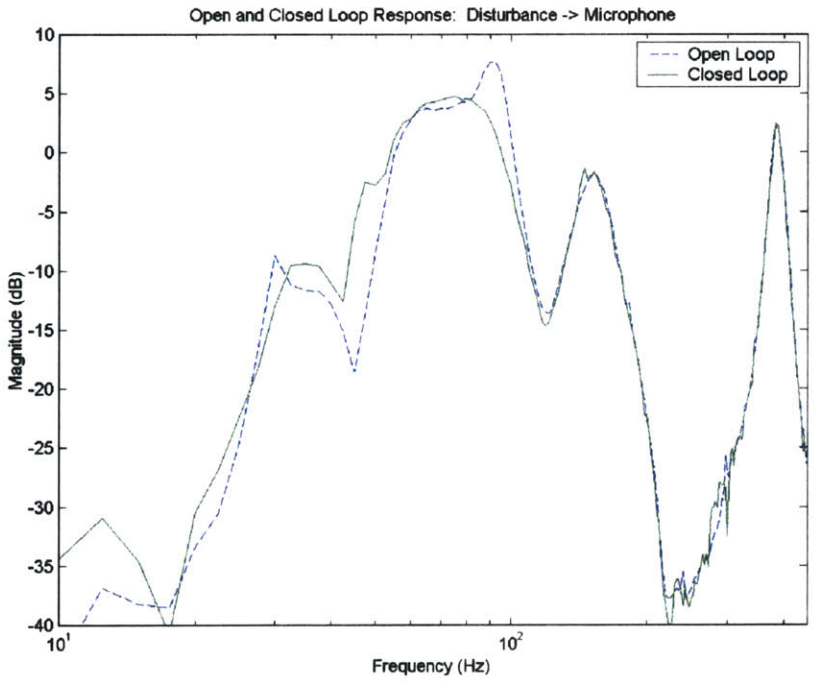

Figure 32: Open and Closed Loop Structural Control at 90 Hz

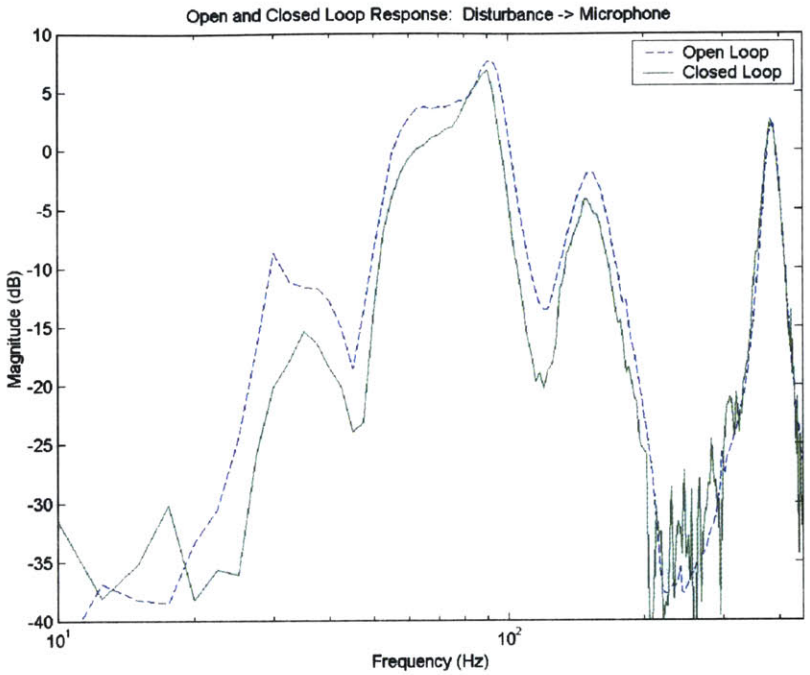

Figure 33: Open and Closed Loop OAUGDP Control at 90 Hz

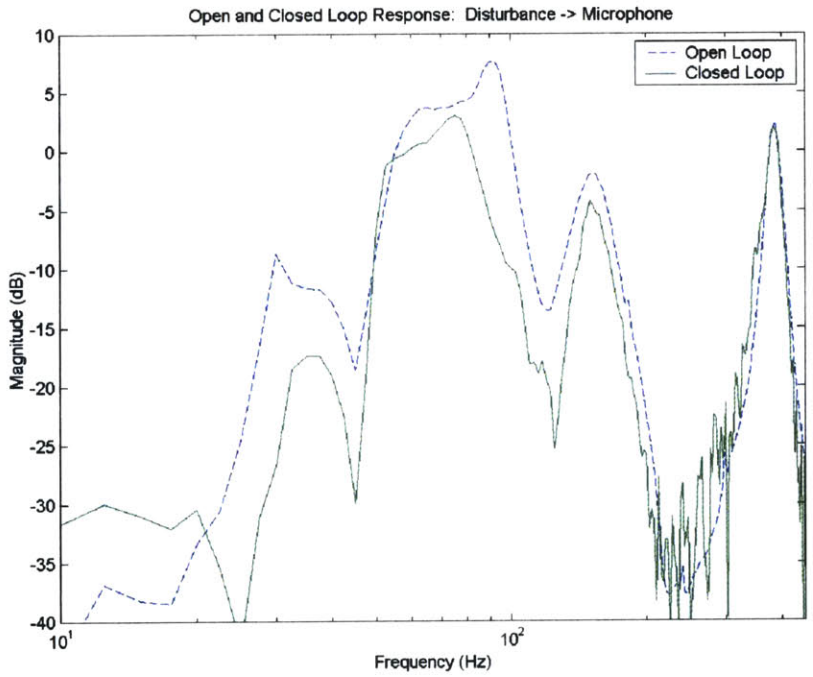

Figure 34: Combined OAUGDP and Structural Control

Figure 34 shows the results of combined control. We see in Figure 34 that the reductions at the first mode are a combination of the reductions from both methods. The results from this experiment are given in Table 5.

Table 5: Combined Structural OAUGDP Control Targeting the Same Mode

Controller	Frequency 90 Hz
Structural Only	4.9 dB
OAUGDP Only	1.3 dB
Combined	13.0 dB

The combined results given in Table 5 indicate a significantly larger increase for the combined controller. The reason for this large reduction is that the reductions from each controller added to one another. However, this does not completely explain why the combined reductions were twice what were expected.

One possibility is that the reductions in Table 5 for the OAUGDP control do not show the maximum reduction for that controller, but rather the reduction at 90 Hz. Reductions at other frequencies of the OAUGDP control were closer to 7 dB, which when added to the structural control would nearly equal the combined results. So, there may be some coupling between the two controllers that shifts the reductions up and down the frequency range.

Another interesting thing to look at is the broadband reductions, which are the eventual goal of any noise reduction method for the launch loads problem. Broadband reductions were calculated over the frequency range from 20 Hz to 200 Hz. These reductions are shown in Table 6.

Table 6: Broadband Reductions for Combined Control (20 Hz to 200 Hz)

Controller	Broadband Reductions
Structural – 90 Hz, OAUGDP – 385 Hz	-0.4 dB
Structural & OAUGDP – 90 Hz	5.9 dB

The negative value in Table 6 indicates an increase rather than a decrease. The controller targeting different modes did not have a desirable broadband result as indicated by Table 6, and as can be seen in the open and closed loop plots for that controller. But, the combined controller targeting the same mode did have good broadband results. One reason for the effectiveness of this controller compared to other may be that the OAUGDP targeted a lower frequency. The lower the target frequency is relative to the plasma generation frequency, means more plasma generated that can be actuated.

Chapter 7

GLOBAL VS. LOCAL REDUCTIONS

7.1 Setup

The desire to have global noise reductions has already been discussed. To determine whether the results presented in the previous section were global or local, a performance microphone was inserted into the PVC cylinder 10 inches from the feedback microphone along the cylinder axis. This microphone was shielded electro-magnetically in the same manner as the feedback microphone.

7.2 Results

The structural controller was run first. This was already known to be a globally-reducing method, so we expected attenuations to show up at the performance microphone as well as the feedback microphone. The results from this test are shown in Figure 35. Figure 35 shows at 90 Hz of 8.2 dB at the feedback microphone and 8.3 dB at the performance microphone. This would indicate that the structural controller does indeed produce global reductions.

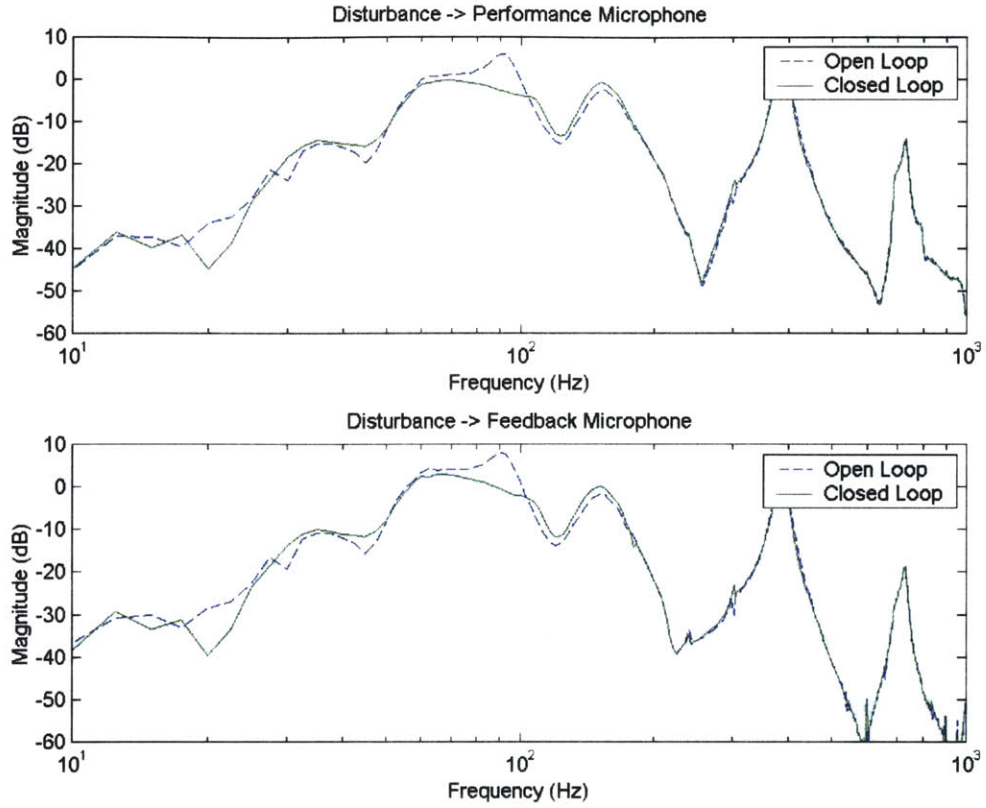

Figure 35: Open and Closed Loop Structural Control at 90 Hz

The global nature of the OAUGDP controller was also evaluated. For the first test, the 385 Hz mode was targeted, and reductions were measured. Since the modal pattern of the OAUGDP electrode grid was not designed for this mode, we did not expect global reductions at this frequency. Figure 36 shows that although the feedback microphone reductions are present, these do not completely show up at the performance microphone location. The reductions are calculated at 385 Hz as 4.5 dB at the feedback microphone and 1.9 dB at the performance microphone.

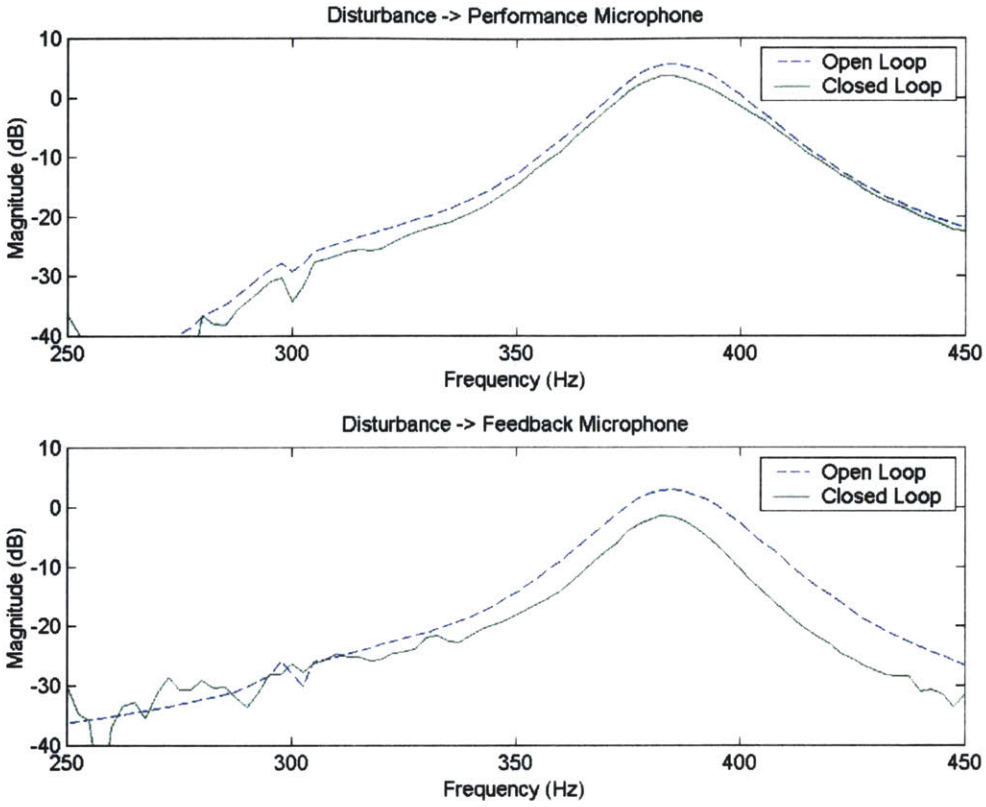

Figure 36: Open and Closed Loop OAUGDP Control at 385 Hz

Finally, the OAUGDP controller was set to target the first structural mode at 90 Hz, for which the modal pattern was designed. Unfortunately, they do not indicate global reductions. Results from this OAUGDP controller are given in Figure 37. Calculated reductions for this test showed a 5.7 dB reduction at the feedback microphone and 3.5 dB at the performance microphone.

Figure 37 shows that the reductions were still not the same at the performance microphone as they were for the feedback microphone. While there were some reductions at the performance microphone, comparison would indicate that the OAUGDP controller was not global in the same sense as the structural controller. The results from these three tests are presented in Table 7.

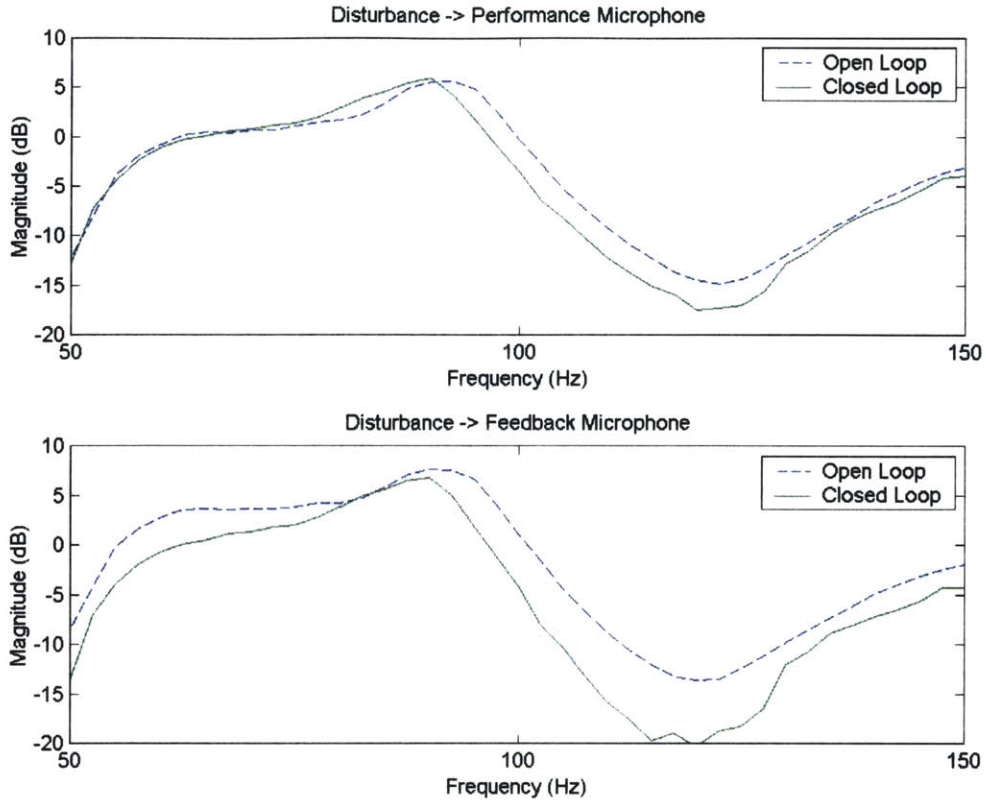

Figure 37: Open and Closed Loop OAUGDP Control at 90 Hz

Table 7: Global Reduction Testing Results

Controller	Performance Microphone	Feedback Microphone
Structural	8.3 dB	8.2 dB
OAUGDP – 385 Hz	1.9 dB	4.5 dB
OAUGDP – 90 Hz	3.5 dB	5.7 dB

Given the results in Table 7 and in the figures in this section, it appears that the OAUGDP, falling into the active noise control category for actuators, does not produce global reductions. Attenuations were observed at the performance microphone, but these could likely be attributed to the proximity to the feedback microphone. The frequencies of interest being fairly low, the associated wavelengths were on the order of a meter, and

the distance between feedback and performance microphone was approximately one-quarter of that wavelength.

The modal pattern did not prove very successful at globally reducing sound, as the global effects did not vary much between the 385 Hz and 90 Hz tests. One possible reason for the poor performance of the modal grid is that while the amount of plasma over the panel surface followed the first modeshape, the amplitude of the field driving the plasma did not follow the same shape. To create a truly modal actuator, the applied electric field should also follow the modeshape. This was beyond the scope of the work done here, and could be considered for future work on the subject.

Chapter 8

CONCLUSIONS

8.1 Conclusions

A panel capable of generating an OAUGDP over its surface was tested as a possible actuator for active noise control problems. Specifically, we were interested in its application to the launch loads attenuation problem. It meets many of the requirements of the launch loads problem, but it did not meet others.

The main requirements of the launch loads problem are weight, cost, control authority, control bandwidth, and global noise reductions. The first two are met by the OAUGDP panel. To modify a payload fairing to have the ability to produce an OAUGDP layer inside, would require less than one ounce of copper per square foot, which is also not very expensive. And, because the copper electrodes can be applied in any orientation, application to the interior of a payload fairing would be possible.

The control bandwidth available is appropriate for the launch loads problem where frequencies over about 500 Hz are attenuated using acoustic blankets. The control authority provided by the OAUGDP is significant, but might need to be improved if it is to be used in launch vehicle fairings. This could be accomplished by increasing the applied electric field to the electrodes, as only an easily attainable voltage level was used for this study.

The fact that the OAUGDP method can be used in conjunction with structural methods makes it even more attractive. Whether or not active methods should be used at all due to the power requirements, is not a matter for this study. But, in terms of power consumption, the OAUGDP requires a similar amount of power to piezoelectric patches. If active methods are believed to be feasible, then OAUGDP methods are viable options.

Where the plasma panels fall short is in the byproducts of plasma generation, and in the lack of global noise reduction. The production of the OAUGDP also yields electro-magnetic interference at radio frequencies. This interference can be dealt with, as seen in the microphones used in the experiments of this study, by shielding with thin layers of metal or metal mesh. Ozone is also produced by the plasma generation process. The levels are such that humans in an enclosed environment would require some preventative measures. Such levels of ozone may also not be desirable for certain payloads due to the reactive nature of ozone.

The real problem with the OAUGDP is that it is an active noise control technology, and therefore does not inherently produce global noise reductions. It may be possible to produce a modal actuator by accurately modeling the acoustic environment, but it was not achieved in the work presented here.

The conclusions then, are that the OAUGDP is a viable active noise control actuator which has shown an ability to provide random noise reductions of as much as 19 dB over a narrowband frequency range, and nearly 6 dB over a broad frequency range. OAUGDP panels can be used in much the same way as standard voice coil speaker, but are extremely light, and can be applied to almost any surface.

In addition, OAUGDP elements can be combined with structural actuators on the same panel to produce a dual control device. While the structural actuator targets reduction of transmission through the panel, the OAUGDP can target interior noise and attempt to further reduce sound. Modal OAUGDP elements can also be produced, however, global control using these elements has not yet been demonstrated.

Drawbacks of OAUGDP usage include EMI and ozone production during operation, but these problems can be dealt with. Future work is required to enable the application of OAUGDP panels or combined OAUGDP structural panels to the launch loads alleviation problem.

8.2 Future Work

Future work in this area might immediately focus on the global versus local reductions issue. Either a modal actuator or distributed actuation might be a consideration for solving that problem, and could be designed in the same way as the modal actuator presented in this work. In the improved design, the ability to have the amplitude of oscillations also follow a modal pattern would be desireable. This could be done by dividing the applied voltage to each ring in the proper proportions. Because the voltage differences between the rings would be much less than the large voltage drop between the cathode and anode, arcing between rings would not be a problem.

Distributed sensing and actuation would also be a possibility for future work. By creating a large array of panels with both structural and OAUGDP elements, it might be possible to actuate on the system modes. Inaccuracies due to placement of modal

actuators are removed in this way. Control using distributed sensing and actuation would require more hardware and computational power.

Along with a modal actuator, it would also be interesting to perform a three-dimensional experiment with an OAUGDP panel, and also with a combined OAUGDP, structural control panel. These tests would also require more hardware and computational power.

References

[1] Glaese, R. M, *Impedance Matching for Structural-Acoustic Control*, Ph.D. thesis, Massachusetts Institute of Technology, Cambridge, MA, Apr. 1997.

[2] Fosness, E. R., "Advanced Mechanisms for Space Applications", *Space Congress Proceedings*, 1997, Canaveral Council of Technical Societies, Cape Canaveral, FL.

[3] Hughes, W. O. and McNelis, A. M., "Cassini/Titan IV Acoustic Blanket Development and Testing", *Proceedings – Annual Technical Meeting of the Institute of Environmental Sciences*, Mount Prospect, IL, 1996, pp. 205-211.

[4] Robinson, M. J., "Composite Structures on the Delta Launch Vehicles", The Boeing Company, Huntington Beach, CA, June, 1998.

[5] Fuller, C. R. and Hansen, C., "Active Control of Interior Noise in Model Aircraft Fuselages Using Piezoceramic Actuators", *Proceedings – 13th AIAA Aeroacoustics Conference, 1990*, AIAA 90-3922.

[6] Thomas, D. R., et al, "Active Control of sound transmission through stiff lightweight composite fuselage constructions", *Proceedings – 14th AIAA Aeroacoustics Conference II*, 1992, pp 552-560.

[7] Pascal, R., *Actuator and Sensor Design and Modeling for Structural Acoustic Control*, M.S. thesis, Massachusetts Institute of Technology, Cambridge, MA, June 1999.

[8] Wong, J. K., *Implementation of Multi-Layer Active Structural-Acoustic Transmission Control*, M.S. thesis, Massachusetts Institute of Technology, Cambridge, MA, June 2001.

[9] Asari, K., *Vibroacoustic Modeling and Control for Launch Vehicle Shrouds*, M.S. thesis, Massachusetts Institute of Technology, Cambridge, MA, June 1998.

[10] Pierce, A. D., *Acoustics: An Introduction to Its Physical Principles and Applications*, Acoustical Society of America, Woodbury, NY, 1989.

[11] Higdon, A.; Ohlsen, E. H.; Stiles, W. B.; Weese, J. A.; Riley, W. F, *Mechanics of Materials*, John Wiley & Sons, New York, NY, 1989.

[12] Anderson, J. D., *Introduction to Flight*, McGraw-Hill, New York, NY, 1989.

[13] Roth, J. R., "Industrial Applications of the One Atmosphere Uniform Glow Discharge Plasma", *IEEE International Conference on Plasma Science*, Piscataway, NJ, 1998, p. 178-179.

[14] Hull, A. J.; Radcliffe, C. J.; Southward, S. C., "Global Active Noise Control of a One-Dimensional Duct Using a Feedback Controller", *Journal of Dynamic Systems Measurement and Control – Transactions of the ASME*, V. 115, no. 3, Sep. 1993, p. 488-494.

[15] Roth, J. R., "Mechanism for a sustained ball lightning glow discharge plasma at one atmosphere pressure", *IEEE International Conference on Plasma Science*, Piscataway, NJ, 1996, p. 151.

[16] Roth, J. R.; Tsai, P. P.; Liu, C.; Laroussi, M.; and Spence, P. D.: "One Atmosphere Uniform Glow Discharge Plasma", U. S. Patent #5,414,324, Issued May 9, 1995.

[17] Roth, J. R., *Industrial Plasma Engineering: Volume 1*, Institute of Physics, Philadelphia, PA, 1995.

[18] Griffiths, D. J., *Introduction to Electrodynamics*, Prentice-Hall, Englewood Cliffs, NJ, 1989.

[19] Gadri, R. B.; Sherman, D. M.; Chen, Z.; Karakaya, F.; Roth, J. R., "One Atmosphere Uniform Glow Discharge Plasma as a classical normal glow discharge", *IEEE International Conference on Plasma Science*, Piscataway, NJ, 1999, p. 201.

[20] Roth, J. R.: "Method and Apparatus for Covering Bodies with a Uniform Glow Discharge Plasma and Applications Thereof". U. S. Patent #5,669,583. Issued Sep. 23, 1997.

[21] Roth, J. R.; Sherman, D. M.; and Wilkinson, Stephen P.: "Boundary Layer Flow Control With a One Atmosphere Uniform Glow Discharge Surface Plasma", AIAA Paper 98-0328, 1998.

[22] Horowitz, H. and Hill, H., *The Art of Electronics*, McGraw-Hill, 1990.

[23] Hirose, A. and Lonngren, K. E., *Introduction to Wave Phenomena*, Krieger Publishing, Malabar, FL, 1991.

[24] Morrison, R., *Grounding and Shielding Techniques in Instrumentation*, John Wiley & Sons, New York, NY, 1986.

[25] Thumann, A. and Miller, R. K., *Fundamentals of Noise Control Engineering*, Fairmont Press, Atlanta, GA, 1986.

[26] Hansen, C. J. and Snyder, S. D., *Active Control of Noise and Vibration*, Chapman and Hall, London, 1997.

[27] Belanger, P. R., *Control Engineering: A Modern Approach*, Saunders College Publishing, Fort Worth, 1995.

[28] Gutierrez, C., *Unidirectional Active Acoustic Control for Launch Vehicle Fairings*, M.S. thesis, Massachusetts Institute of Technology, Cambridge, MA, Nov. 2000.

[29] Rao, J. S, *Dynamics of Plates*, Narosa Publishing House, New Dehli, 1999.

[30] Harper, C. A., *Handbook of Plastics, Elastomers, and Composites*, McGraw-Hill, New York, NY, 1996.

[31] Meirovitch, L., *Principles and Techniques of Vibrations*, Prentice Hall, Upper Saddle River, NJ, 1997.

[32] Hagood, N. W.; Chung, W. H.; Flotow, A., "Modeling of Piezoelectric Actuator Dynamics for Active Structural Control", *Journal of Intelligent Material Systems and Structures*, V. 1, July, 1990, p. 327-354.

[33] Hagood, N. W. and Von Flotow, A., "Damping of Structural Vibrations with Piezoelectric Materials and Passive Electrical Networks", *Journal of Sound and Vibration*, V. 146, no. 2, 1991, p. 243-268.